8-Oxoguanine causes neurodegeneration during MUTYH-mediated DNA base excision repair

Zijing Sheng,[1,2] Sugako Oka,[1,2] Daisuke Tsuchimoto,[1,2] Nona Abolhassani,[1] Hiroko Nomaru,[1] Kunihiko Sakumi,[1,2] Hidetaka Yamada,[1,3] and Yusaku Nakabeppu[1,2]

[1]Division of Neurofunctional Genomics, Department of Immunobiology and Neuroscience, Medical Institute of Bioregulation, and [2]Research Center for Nucleotide Pool, Kyushu University, Fukuoka, Japan. [3]Cognitive and Molecular Research Institute of Brain Diseases, Kurume University School of Medicine, Kurume, Japan.

8-Oxoguanine (8-oxoG), a common DNA lesion caused by reactive oxygen species, is associated with carcinogenesis and neurodegeneration. Although the mechanism by which 8-oxoG causes carcinogenesis is well understood, the mechanism by which it causes neurodegeneration is unknown. Here, we report that neurodegeneration is triggered by MUTYH-mediated excision repair of 8-oxoG–paired adenine. Mutant mice lacking 8-oxo–2′-deoxyguanosine triphosphatase–depleting (8-oxo–dGTP–depleting) MTH1 and/or 8-oxoG–excising OGG1 exhibited severe striatal neurodegeneration, whereas mutant mice lacking MUTYH or OGG1/MUTYH were resistant to neurodegeneration under conditions of oxidative stress. These results indicate that OGG1 and MTH1 are protective, while MUTYH promotes neurodegeneration. We observed that 8-oxoG accumulated in the mitochondrial DNA of neurons and caused calpain-dependent neuronal loss, while delayed nuclear accumulation of 8-oxoG in microglia resulted in PARP-dependent activation of apoptosis-inducing factor and exacerbated microgliosis. These results revealed that neurodegeneration is a complex process caused by 8-oxoG accumulation in the genomes of neurons and microglia. Different signaling pathways were triggered by the accumulation of single-strand breaks in each type of DNA generated during base excision repair initiated by MUTYH, suggesting that suppression of MUTYH may protect the brain under conditions of oxidative stress.

Introduction

The DNA and precursor nucleotides in living organisms are always in danger of oxidation by ROS that are inevitably generated as a by-product of oxygen respiration and are products of host defense and signal transduction mechanisms (1, 2). If oxidized lesions accumulate in DNA, mutagenesis or cell death may result (3–5). Among all nucleobases, guanine is known to be the most susceptible to oxidation, and its simple oxidized form, 8-oxoguanine (8-oxoG), which can pair with adenine as well as cytosine, is one of the major oxidation products in DNA and nucleotides (6, 7).

Mammalian cells are equipped with elaborate means of minimizing accumulation of 8-oxoG in DNA. 8-oxo–2′-deoxyguanosine triphosphatase (8-oxo–dGTPase) encoded by *MTH1* hydrolyzes 8-oxo–dGTP to 8-oxo–dGMP and pyrophosphate in nucleotide pools, thereby avoiding incorporation of 8-oxo–dGMP into DNA (8, 9). 8-OxoG DNA glycosylase 1 encoded by *OGG1* excises 8-oxoG paired with cytosine in DNA (10), while adenine DNA glycosylase encoded by *MUTYH* removes the adenine inserted opposite 8-oxoG in template DNA during DNA replication (11), thus preventing mutagenesis. Mutant mice lacking these genes exhibit increased spontaneous mutation rate and susceptibility to carcinogenesis with increased accumulation of 8-oxoG in DNA (12–15).

Oxidative stress is considered to be important in the etiology of several neurodegenerative disorders, and it has been shown that 8-oxoG levels are significantly increased in mitochondrial DNA (mtDNA) as well as nuclear DNA (nDNA) in the brains of patients with Parkinson's disease (PD) (16), Alzheimer's disease (AD) (17), and Huntington's disease (HD) (18) in comparison with control brains. Expression levels of MTH1, OGG1, and MUTYH are also significantly altered in the brains of such patients (16, 19–22), suggesting that their altered expression along with accumulation of 8-oxoG in brain cause neurodegeneration; however, how 8-oxoG and these enzymes are associated with the neurodegenerative process is poorly understood.

The striatum plays a key role in motor, cognitive, and motivational processes (23). Abnormal striatal function is involved in several neurodegenerative disorders, such as PD, AD, and HD. The inhibitor of mitochondrial succinate dehydrogenase 3-nitropropionic acid (3-NP), a naturally occurring plant toxin, has been shown to cause striatal degeneration and motor impairments in animals similar to those seen in HD (24, 25). It has been established that administration of 3-NP to rodents and nonhuman primates replicates most of the clinical and pathophysiological hallmarks of HD, including spontaneous choreiform and dystonic movements, frontal-type cognitive deficits, and progressive heterogeneous striatal degeneration, at least partially by apoptosis (26). We have shown that increased expression of human MTH1 in mouse striatum efficiently suppresses such striatal degeneration, accompanied by effective suppression of the 8-oxoG accumulation in the striatum induced by 3-NP (27). However, it is not clear to what extent 8-oxoG accumulated in DNA is responsible for the neurodegeneration, because MTH1 can hydrolyze oxidized forms of ATP, GTP, and dATP as well as dGTP (28). Moreover, it is not known which type of DNA (nDNA and/or mtDNA) harboring 8-oxoG is associated with such neurodegeneration, nor is it known how the neuronal loss occurs.

Conflict of interest: The authors have declared that no conflict of interest exists.
Citation for this article: *J Clin Invest.* doi:10.1172/JCI65053.

In the present study, we investigated the mechanism by which 8-oxoG is involved in neurodegeneration using mutant mice lacking *Ogg1*, *Mth1*, and/or *Mutyh* genes under conditions of oxidative stress. We demonstrated that OGG1 cooperatively protects brain with MTH1, reflecting a beneficial role of DNA repair and, intriguingly, that DNA repair by MUTYH is required for neurodegeneration upon 8-oxoG accumulation in brain, thus exhibiting a harmful role of DNA repair.

Results

Mth1/Ogg1-double-KO mice are highly vulnerable to striatal degeneration caused by chronic exposure to 3-NP. We first immunohistochemically confirmed the expression of MTH1 and OGG1 proteins in mouse striatum. Specific immunoreactivities (IRs) for both MTH1 and OGG1 were detected only in WT striatum, but not in *Mth1-KO* or *Ogg1-KO* striatum, respectively (Supplemental Figure 1; supplemental material available online with this article; doi:10.1172/JCI65053DS1). Immunofluorescence microscopy revealed that cytoplasmic IRs for MTH1 and OGG1 were predominantly detected in DARPP32-positive medium spiny neurons (MSNs) in WT striatum (Figure 1A). Immunoelectron microscopy confirmed that MTH1 and OGG1 IRs were distributed in the cytoplasm and nucleus only in the WT striatum (Supplemental Figure 2). It is evident that the OGG1 cytoplasmic IR colocalized with mitochondrial HSP60 IR (Figure 1A). Thus, we hypothesized that MTH1 and OGG1 play important roles in protecting MSNs in the striatum from oxidative stress.

To evaluate this hypothesis, we examined the effects of 3-NP on motor function in WT and mutant mouse strains lacking *Ogg1* and/or *Mth1* genes, in small cohorts (Supplemental Figure 3). Chronic exposure of mice to 3-NP resulted in motor impairments. Individual pairwise comparisons to WT mice revealed that *Mth1/Ogg1*–double-KO (*Mth1/Ogg1*-DKO) and to a lesser extent *Ogg1*-KO mice exhibited a statistically significant decline of travel distance in an open-field test, but no significant difference was found between *Mth1*-KO and WT mice ($P < 0.05$, $P < 0.02$, respectively). We then examined the effects of 3-NP on WT and *Mth1/Ogg1*-DKO mice in large cohorts. First, we evaluated the 3-NP–induced motor symptoms in WT and *Mth1/Ogg1*-DKO mice based on neurological scores (refs. 29, 30, and Supplemental Figure 4) and found that *Mth1/Ogg1*-DKO mice exhibited more severe motor symptoms. A quantitative analysis of spontaneous locomotor behavior in their home cages during day and night revealed that *Mth1/Ogg1*-DKO mice show more hypolocomotor activity in the home cages during the night on the fifth and sixth days of 3-NP exposure (Supplemental Figure 5). An open-field test showed that the distance travelled by DKO mice in the open field was significantly reduced, to 52% of the level seen in WT mice after exposure to 3-NP for 7 days, and vertical rearing was also significantly reduced in DKO mice to 59% of the level seen in WT mice (Figure 1B and Supplemental Videos 1 and 2). *Mth1/Ogg1*-DKO and WT mice both exhibited modest reductions in performance on a rotarod test after exposure to 3-NP for 7 days; however, there was no significant difference between the 2 groups of mice (data not shown), indicating that the significantly decreased motor activity in *Mth1/Ogg1-DKO* mice was not due to increased muscle disorder.

More severe striatal degeneration was observed in DKO mice than in WT mice after 7 days of exposure to 3-NP (Figure 1C). Laser scanning confocal immunofluorescence microscopy (LSCIM) revealed that most DARPP32-positive MSNs were lost and increased numbers of F4/80-positive microglia were detected in the DKO striatum, especially in the dorsolateral part of the striatum, after exposure to 3-NP for 7 days (Figure 1D), indicating that the 3-NP induces striatal degeneration accompanied by microgliosis. Thus, we concluded that the double deficiency in MTH1 and OGG1 renders the striatum highly vulnerable to 3-NP–induced neurodegeneration.

Significant increase in the level of mitochondrial 8-oxoG, but not nuclear 8-oxoG, in the Mth1/Ogg1-DKO striatum after exposure to 3-NP. We previously established that 8-oxoG in mtDNA can be visualized in tissue sections treated only with RNase before incubation with anti–8-oxo–dG, while 8-oxoG in nDNA can be detected in sections treated with RNase and HCl before incubation with the antibody (31, 32). Most neurons in the DKO striatum were lost after exposure to 3-NP for 7 days (Figure 1, C and D); therefore, it is likely that 8-oxoG in nDNA may not be detected in the striatum after 7 days of exposure to 3-NP. We found that MSNs expressing DARPP32 were still detectable in the striata of WT and DKO mice after exposure to 3-NP for 4 days (Figure 2A); therefore, we examined nuclear 8-oxoG levels by LC-MS/MS analysis of striatal nDNA prepared after exposure to 3-NP for 1 or 3 days using stable isotope-labeled [^{15}N5] 8-oxo–dG as an internal standard. Nuclear 8-oxo–dG levels were not significantly increased in either group after exposure to 3-NP, although DKO mice had higher basal levels of nuclear 8-oxo–dG in the striatum than did WT mice (Figure 2B). LSCIM following pretreatment of sections with HCl revealed that exposure to 3-NP for 4 days causes a marginal increase in nuclear 8-oxoG IR in the DKO striatum in agreement with the results of LC-MS/MS analysis (data not shown). These results indicate that 8-oxoG is not highly accumulated in nDNA prior to loss of MSNs in the striatum.

Exposure to 3-NP for 7 days caused significant increases in cytoplasmic 8-oxoG IR in the *Mth1/Ogg1*-DKO striatum in comparison with WT or untreated samples without HCl pretreatment, suggesting 8-oxoG accumulation in mtDNA (Figure 3, A and B). LSCIM revealed that DARPP32-positive MSNs in the DKO striatum exhibited strong cytoplasmic 8-oxoG IR without HCl pretreatment after exposure to 3-NP for 4 days (Figure 3C) and that this IR was colocalized with that for mitochondrial transcription factor A (TFAM) with which mtDNA is packaged (ref. 33 and Figure 3D), indicating that 8-oxoG accumulates mostly in the mtDNA of MSNs in the DKO striatum. The basal level of mitochondrial 8-oxoG in DKO MSNs was 8-fold higher than that in WT MSNs without exposure to 3-NP, indicating an increased spontaneous accumulation of 8-oxoG in the mtDNA. After 4 days of 3-NP exposure, the levels were significantly increased in both WT and DKO MSNs; the level in DKO MSNs was 3.5 times higher than that in WT MSNs (Figure 3, E and F).

On the seventh day of exposure to 3-NP, we observed significantly increased IR for single-stranded DNA (ssDNA) in the cytoplasm of neurons in the DKO striatum, in agreement with selective damage such as single-strand breaks (SSBs) in their mtDNA. Cells with small nuclei exhibited nuclear ssDNA IRs (Figure 3G), indicating that the nuclei of microglia also accumulate DNA damage. On the seventh day of exposure to 3-NP, we noticed that microglia proliferating in the region of striatum, where MSNs were largely lost, exhibit nuclear, and to a lesser extent cytoplasmic, 8-oxoG IR (Figure 3H).

Independent activation of calpain and apoptosis-inducing factor during the striatal degeneration caused by 3-NP. We previously showed that *Ogg1*-KO cells expressing a nuclear form of human OGG1 accumulate 8-oxoG selectively in mtDNA under oxidative stress and

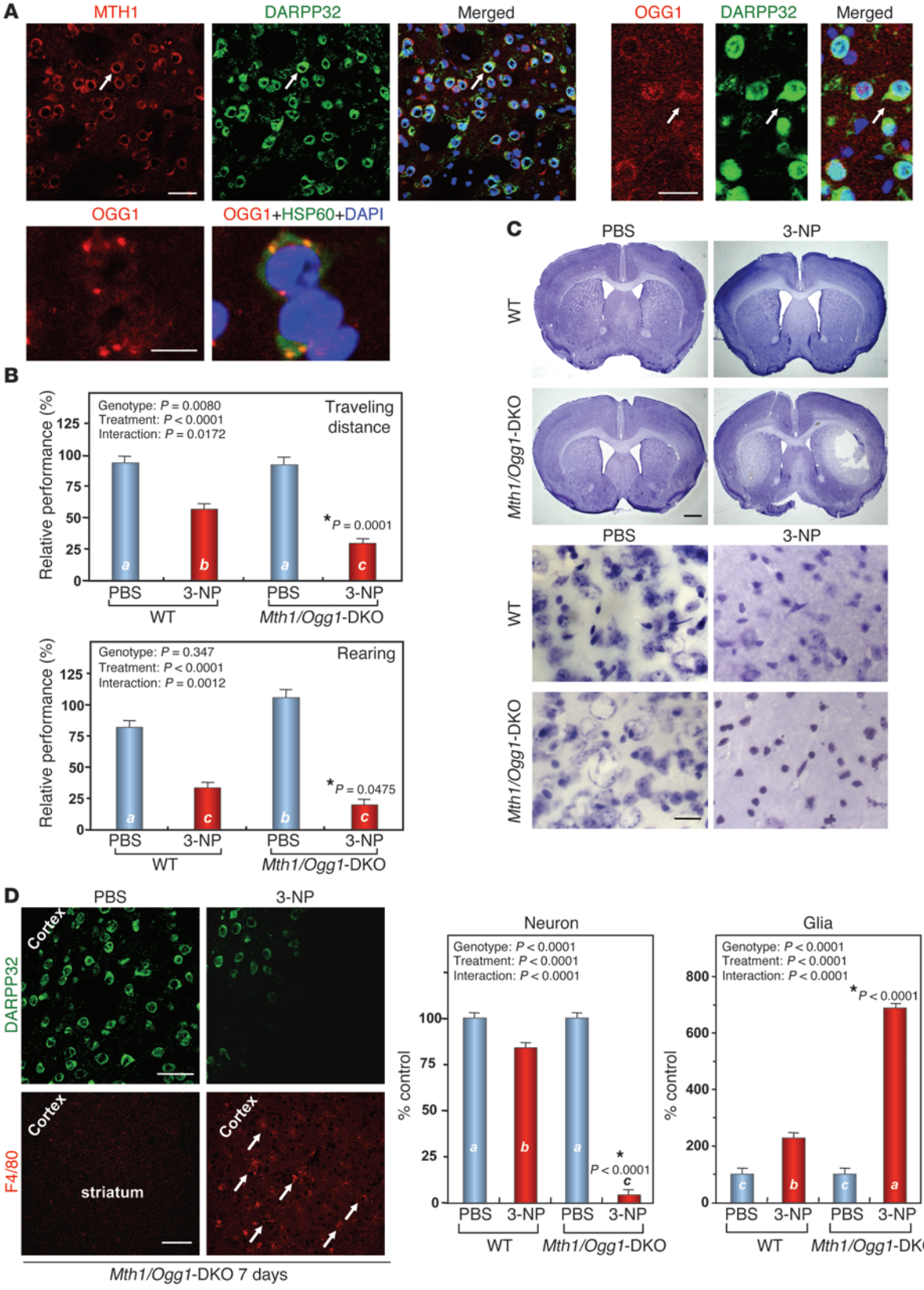
A
MTH1
DARPP32
Merged
OGG1
DARPP32
Merged
OGG1
OGG1+HSP60+DAPI
B
Genotype: P = 0.0080
Treatment: P < 0.0001
Interaction: P = 0.0172
Traveling distance
Relative performance (%)
*P = 0.0001
PBS
3-NP
PBS
3-NP
WT
Mth1/Ogg1-DKO
Genotype: P = 0.347
Treatment: P < 0.0001
Interaction: P = 0.0012
Rearing
*P = 0.0475
C
PBS
3-NP
WT
Mth1/Ogg1-DKO
D
PBS
3-NP
DARPP32
F4/80
Cortex
striatum
Mth1/Ogg1-DKO 7 days
Neuron
Glia
Genotype: P < 0.0001
Treatment: P < 0.0001
Interaction: P < 0.0001
% control
*P < 0.0001

Figure 1
Mth1/Ogg1-DKO mice are extremely vulnerable to 3-NP–induced motor impairments and striatal degeneration. (**A**) MTH1 (upper left panels) and OGG1 (upper right panels) IRs (red) were abundant in WT striatum and were predominantly localized in DARPP32-positive neurons (green). Arrows show positively stained neurons. Scale bar: 20 μm. OGG1 IR (red) in the cytoplasm colocalized with HSP60 IR (green) (lower panels). Scale bar: 10 μm. (**B**) Motor impairments after exposure to 3-NP. Numbers of animals examined per condition are 14 (WT, PBS), 21 (WT, 3-NP), 11 (*Mth1/Ogg1*-DKO, PBS), and 22 (*Mth1/Ogg1*-DKO, 3-NP). (**C**) Striatal degeneration as revealed by Nissl staining. Upper panels, lower magnification; scale bar: 1 mm. Lower panels: higher magnification, scale bar: 20 μm. (**D**) Loss of MSNs expressing DARPP32 (green) and microgliosis as detected by F4/80 (red) staining. Arrows indicate F4/80-positive microglia. The numbers of neurons and glia in the dorsolateral striatum were counted on Nissl-stained sections, $n = 3$ for each group. Scale bars: 20 μm (upper); 100 μm (lower). In **B** and **D**, data in each bar graph are shown with LS means ± SEM, and *P* values for the effects of genotype, treatment, and interaction between genotype, and treatment are shown. Levels not connected with the same letter are significantly different (Tukey's HSD test). **P*, compared with WT mice exposed to 3-NP.

demonstrated that the accumulation of 8-oxoG in mtDNA causes mitochondrial dysfunction and Ca^{2+} release, thereby activating calpain to execute caspase-independent cell death (34). Because 8-oxoG was selectively accumulated in the mtDNA of MSNs in *Mth1/Ogg1*-DKO striatum after 3-NP exposure (Figure 3, A–F), we examined whether accumulation of 8-oxoG in mtDNA in the striatum activates calpain. Western blotting analysis of α-spectrin, a substrate for calpain (35), revealed that 3-NP exposure for 4 or 7 days caused markedly increased processing of α-spectrin in the *Mth1/Ogg1*-DKO striatum in comparison with WT (Figure 4A). The relative level of a 145-kDa band corresponding to a major calpain-cleaved product (35) was significantly increased in the DKO striatum after exposure to 3-NP, while such increased cleavage of α-spectrin was barely seen in WT striatum (Figure 4A). It is likely that the dose of 3-NP (120 mg/kg/d) is not enough to activate calpain in WT striatum, thereby causing little neurodegeneration (Figure 1), consistent with a previous suggestion that the activation of calpain observed in 3-NP–treated animals is probably instrumental in striatal degeneration (36). In PBS-treated striatum, α-spectrin IR was detected in the nuclei of neurons in both WT and DKO striatum; however, we noticed that perinuclear IR for α-spectrin was evident in the DKO striatum after exposure to 3-NP for 4 days (Figure 4B), indicating that the calpain-dependent processing of α-spectrin results in its altered intracellular localization (37). Because such perinuclear IR of α-spectrin was exclusively detected in DARPP32-positive neurons in the DKO striatum after exposure to 3-NP, calpain must be selectively activated in MSNs (Figure 4C).

Using *Ogg1*-KO cells, which express a mitochondrial form of human OGG1, we previously demonstrated that the selective accumulation of 8-oxoG in nDNA causes PARP-dependent nuclear translocation of apoptosis-inducing factor (AIF) and that the cells subsequently underwent PARP/AIF-dependent cell death (34). We therefore examined whether PARP and AIF are involved in 3-NP–induced striatal degeneration. LSCIM with anti-poly(ADP-ribose) (anti-PAR) or anti-AIF antibodies revealed a significant accumulation of PAR-polymer and AIF in the striatal region of DKO mice from which MSNs were largely lost after exposure to 3-NP for 7 days (Figure 4D). We observed increased numbers of F4/80-positive microglia in this region (Figure 1D), and IRs for PAR and AIF were mostly detected in the nuclei of microglia (Figure 5A). No AIF or PAR IR was seen in MSNs (Figure 5B), and no AIF IR was seen in GFAP-positive astrocytes after exposure to 3-NP (Figure 5C). Western blotting analysis of AIF revealed that exposure to 3-NP for 7 days caused significant accumulation of a 57-kDa form of AIF, a processed nuclear form of AIF (38), only in the DKO striatum, but not in the WT striatum (Figure 5D), indicating that delayed activation of AIF accompanied by PAR-polymer accumulation occurs selectively in microglia in the DKO striatum exposed to 3-NP. These data indicate that activation of calpain is restricted to MSNs and that activation of AIF is restricted to microglia.

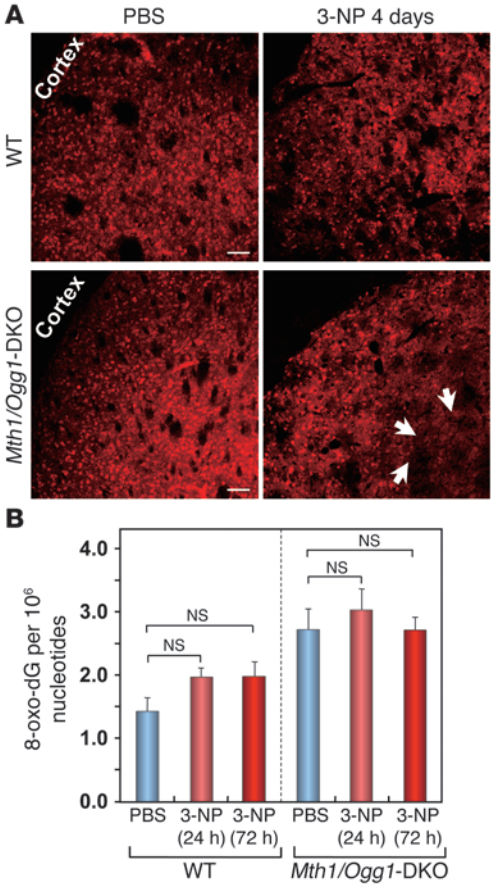

Figure 2
Nuclear 8-oxo–dG levels in striatum detected by LC-MS/MS analysis. (**A**) DARPP32-positive MSNs were still detected on the fourth day of 3-NP exposure. Arrows show that DARPP32 staining was slightly decreased in the *Mth1/Ogg1*-DKO striatum compared with WT striatum exposed to 3-NP. Scale bar: 50 μm. (**B**) Nuclear 8-oxo–dG levels in striatum measured by LC-MS/MS analysis. The number of animals examined is 5 for each group. Residues of 8-oxo–dG per 10^6 nucleotides in nuclear DNA determined by LC-MS/MS are shown as LS means ± SEM. Nuclear 8-oxo–dG levels were not significantly increased in either group after exposure to 3-NP (Student's *t* test).

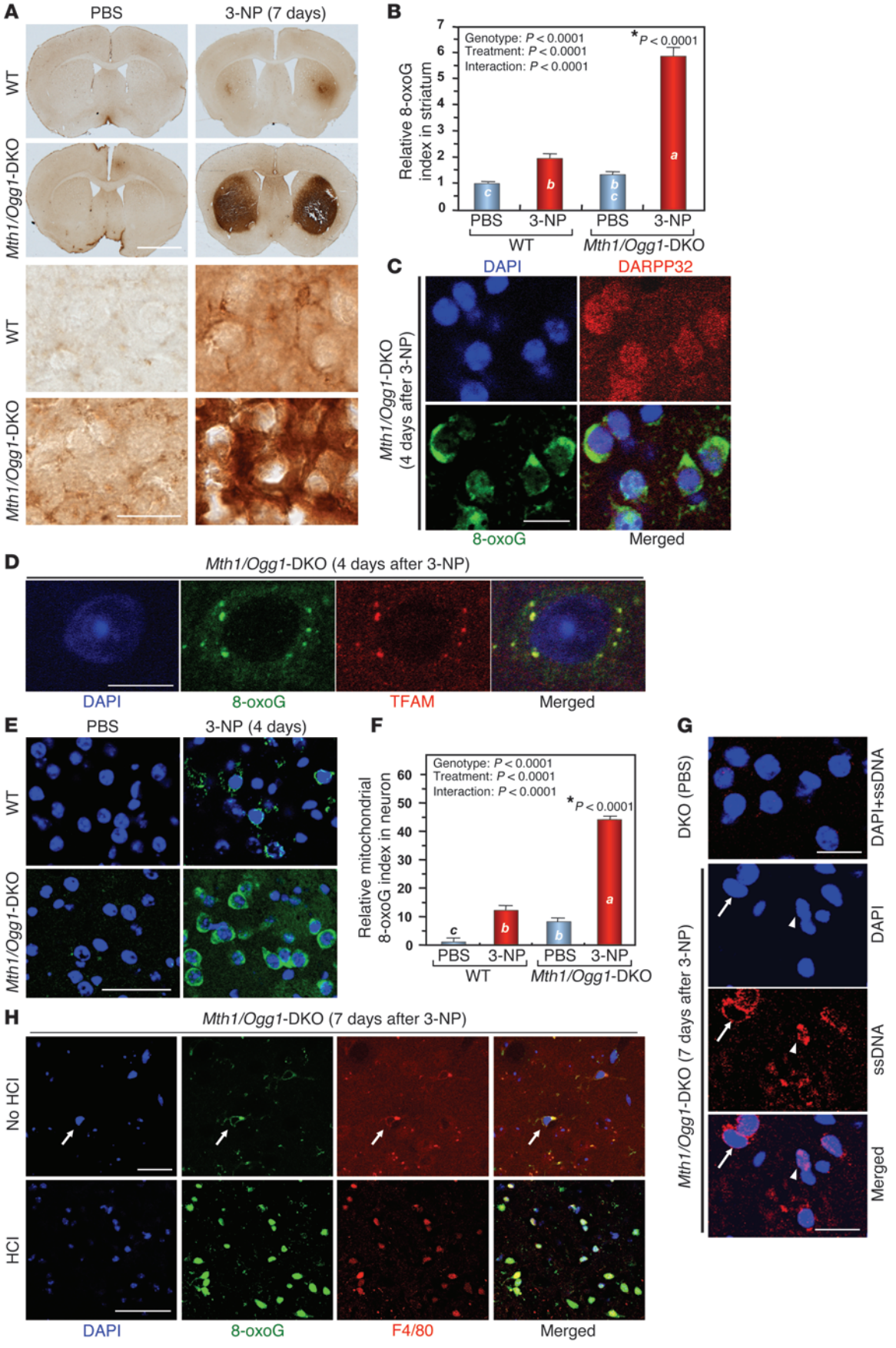
A
PBS
3-NP (7 days)
WT
Mth1/Ogg1-DKO
WT
Mth1/Ogg1-DKO
B
Relative 8-oxoG index in striatum
Genotype: P < 0.0001
Treatment: P < 0.0001
Interaction: P < 0.0001
*P < 0.0001
PBS
3-NP
PBS
3-NP
WT
Mth1/Ogg1-DKO
C
DAPI
DARPP32
Mth1/Ogg1-DKO (4 days after 3-NP)
8-oxoG
Merged
D
Mth1/Ogg1-DKO (4 days after 3-NP)
DAPI
8-oxoG
TFAM
Merged
E
PBS
3-NP (4 days)
WT
Mth1/Ogg1-DKO
F
Relative mitochondrial 8-oxoG index in neuron
Genotype: P < 0.0001
Treatment: P < 0.0001
Interaction: P < 0.0001
*P < 0.0001
PBS
3-NP
PBS
3-NP
WT
Mth1/Ogg1-DKO
G
DKO (PBS)
DAPI+ssDNA
Mth1/Ogg1-DKO (7 days after 3-NP)
DAPI
ssDNA
Merged
H
Mth1/Ogg1-DKO (7 days after 3-NP)
No HCl
HCl
DAPI
8-oxoG
F4/80
Merged

Figure 3
Mth1/Ogg1-DKO striatum exhibits significantly increased accumulation of 8-oxoG in MSNs and microglia after exposure to 3-NP. (**A**) DKO mice exhibited stronger cytoplasmic 8-oxoG IR in the striatum compared with WT mice. Sections were pretreated only with RNase. Upper panels: lower magnification, scale bar: 2 mm. Lower panels: higher magnification. Images were obtained using differential interference contrast (DIC) microscopy, scale bar: 20 μm. (**B**) Quantitative measurement of 8-oxoG IR in the striatum shown in **A** (n = 8 for each group). (**C**) Cytoplasmic 8-oxoG IR was detected in DARPP32-positive neurons. Scale bar: 20 μm. (**D**) Colocalization of the cytoplasmic 8-oxoG IR and TFAM IR. Scale bar: 10 μm. (**E**) Significantly increased mitochondrial 8-oxoG IR in DKO striatum exposed to 3-NP. Scale bar: 50 μm. (**F**) Quantitative measurement of the mitochondrial 8-oxoG IR in neuron. WT (PBS, n = 4; 3-NP, n = 4); DKO mice (PBS, n = 4; 3-NP, n = 5). (**G**) Detection of ssDNA IRs in either nuclei or cytoplasm. Arrow, cytoplasmic ssDNA IR; arrowhead, nuclear ssDNA IR. Scale bar: 20 μm. (**H**) Detection of stronger nuclear 8-oxoG IR in DKO striatal microglia. Nuclear 8-oxoG IR in RNase/HCl-pretreated sections (HCl), and to a lesser extent, cytoplasmic 8-oxoG IR in RNase-pretreated sections (no HCl) were detected in microglia. Scale bars: 20 μm (upper); 50 μm (lower). In **B** and **F**, data are shown as LS means ± SEM. Levels not connected with the same letter are significantly different (Tukey's HSD test). *P, compared with WT mice exposed to 3-NP.

Calpain as well as PARP inhibitors suppress striatal neurodegeneration and improve behavioral impairments induced by 3-NP. We next tested whether inhibition of calpain and PARP could afford neuroprotection against the neurodegeneration following 3-NP administration, to confirm the involvement of the 2 distinct pathways in 3-NP–induced neurodegeneration.

We examined the effects of administration of a calpain inhibitor (MDL28170) and an inhibitor of PARP (3-aminobenzamide [3-AB]) on striatal degeneration induced by 3-NP. Both inhibitors significantly improved 3-NP–induced motor impairments (Figure 6A) and suppressed MSN loss (Figure 6, B and C) as well as microgliosis (Figure 6D) in *Mth1/Ogg1*-DKO mice. The perinuclear distribution of α-spectrin was suppressed by the calpain inhibitor (Figure 6E), while accumulation of both PAR polymer and nuclear AIF was efficiently suppressed by the PARP inhibitor (Figure 6F). Thus, both calpain activation in MSNs and poly(ADP-ribosyl)ation causing nuclear translocation of AIF in microglia play important roles in 3-NP–induced striatal degeneration. Previous research has shown that downregulation of PARP in microglia protects neurons from secondary damage as well as preventing microgliosis following N-methyl-D-aspartate-induced hippocampal injury (39), as we observed for 3-NP–induced striatal degeneration (Figure 6C).

3-NP causes early accumulation of SSBs in mtDNA accompanied by calpain activation in striatal MSNs and delayed accumulation of SSBs in nDNA followed by activation of the PARP/AIF pathway in striatal microglia. Buildup of SSBs in either mtDNA or nDNA was found in *Mth1/Ogg1*-DKO striatum after exposure to 3-NP (Figure 3G). SSBs in nDNA are recognized by PARP, thus facilitating their repair or inducing nuclear translocation of AIF if SSBs are accumulated beyond the repair capacity, while buildup of excessive SSBs in mtDNA is known to cause mitochondrial dysfunction followed by calpain activation (34). We therefore examined the time course and spatial distribution of ssDNA IRs in comparison with those of α-spectrin or PAR IRs in DKO mice after exposure to 3-NP to delineate their interrelation.

LSCIM with an anti-ssDNA antibody revealed that IR for cytoplasmic ssDNA was prominent in the *Mth1/Ogg1*-DKO striatum in comparison with WT mice after 4 days of 3-NP exposure, while nuclear IR for ssDNA was more dominant in the striatal region where MSNs were largely lost after 7 days of 3-NP exposure (Figure 7, A and B). PAR IR was detected only in the DKO striatum exposed to 3-NP for 7 days and mostly colocalized with nuclear ssDNA IR (Figure 7C). On the other hand, cytoplasmic ssDNA IR was detected in neurons with perinuclear α-spectrin IRs (Figure 7D). These observations strongly suggest that 8-oxoG accumulated in either mtDNA in MSNs or nDNA in microglia causes accumulation of SSBs in each type of DNA, and that accumulation of SSBs in mtDNA results in calpain activation in MSNs, while that in nDNA activates the PARP/AIF pathway in microglia.

MUTYH deficiency renders mice resistant to the mitochondrial neurotoxicity of 3-NP. We previously demonstrated that MUTYH-dependent base excision repair (BER) is responsible for the accumulation of SSBs in nDNA or mtDNA with increased 8-oxoG accumulation in *Ogg1*-KO cells (34). To analyze the function of MUTYH in the striatum, we next examined the expression of MUTYH protein in striatum (Figure 8A) and found that MUTYH IR was preferentially localized to the cytoplasm and mitochondria and to a lesser extent nuclei in MSNs (Figure 8, B and C), while nuclear MUTYH IR in microglia was more apparent than that in MSNs (Figure 8D).

When we challenged *Mutyh*-KO mice with various doses of 3-NP (120 mg/kg/d to 180 mg/kg/d), we found that *Mutyh*-KO mice exhibit higher survival rates than do WT mice within 7 days of exposure (data not shown). 3-NP–induced motor symptoms were evaluated in WT and *Mutyh*-KO mice after exposure to 3-NP (150 mg/kg/d) (Supplemental Figure 6), and WT mice exhibited higher scores than did *Mutyh*-KO mice. Furthermore, we examined motor function of the survivors in the open-field test (Figure 8E). *Mutyh*-KO mice exhibited significantly better rearing performance after exposure to 3-NP (120 mg/kg/d) than did WT. Electron microscopic examination and histochemical detection of cytochrome *c* oxidase activity revealed that mitochondrial structure and function were well maintained in the *Mutyh*-KO striatum after 3-NP exposure, while mitochondria in the WT striatum were largely degenerated and exhibited lower cytochrome *c* oxidase activity than did those in the *Mutyh*-KO striatum (Figure 8, F and G), indicating that MUTYH enhances neurodegeneration.

MUTYH-initiated BER mediates 3-NP–induced neurodegeneration. We previously reported that exposure to sodium nitroprusside causes cell death accompanied by 8-oxoG accumulation in the mtDNA of quiescent MTH1-null cells and that knockdown of MUTYH in quiescent MTH1-null cells significantly prevents cell death (40). Considering this finding together with the *Mutyh*-KO phenotype, it is reasonable to assume that striatal degeneration accompanied by calpain and PARP/AIF pathways in *Ogg1*-KO or *Ogg1/Mth1*-DKO mice may be rescued by MUTYH deficiency. Because *Ogg1/Mth1/Mutyh*–triple KO mice are highly susceptible to spontaneous tumorigenesis within 100 days after birth (our unpublished observation), we tested our hypothesis using *Ogg1*-KO and *Ogg1/Mutyh*-DKO mice. *Ogg1/Mutyh*-DKO mice exhibited significantly better motor performance than did *Ogg1*-KO mice after exposure to 3-NP for 7 days (Figure 9A), and neither MSN loss nor microgliosis was evident in the DKO striatum (Figure 9, B and C). IR for nuclear and cytoplasmic ssDNA was again evident in the *Ogg1*-KO striatum after exposure to 3-NP; however, there was no such IR in the *Ogg1/Mutyh*-DKO striatum (Figure 10, A and B). In the *Ogg1*-KO striatum, cytoplasmic ssDNA

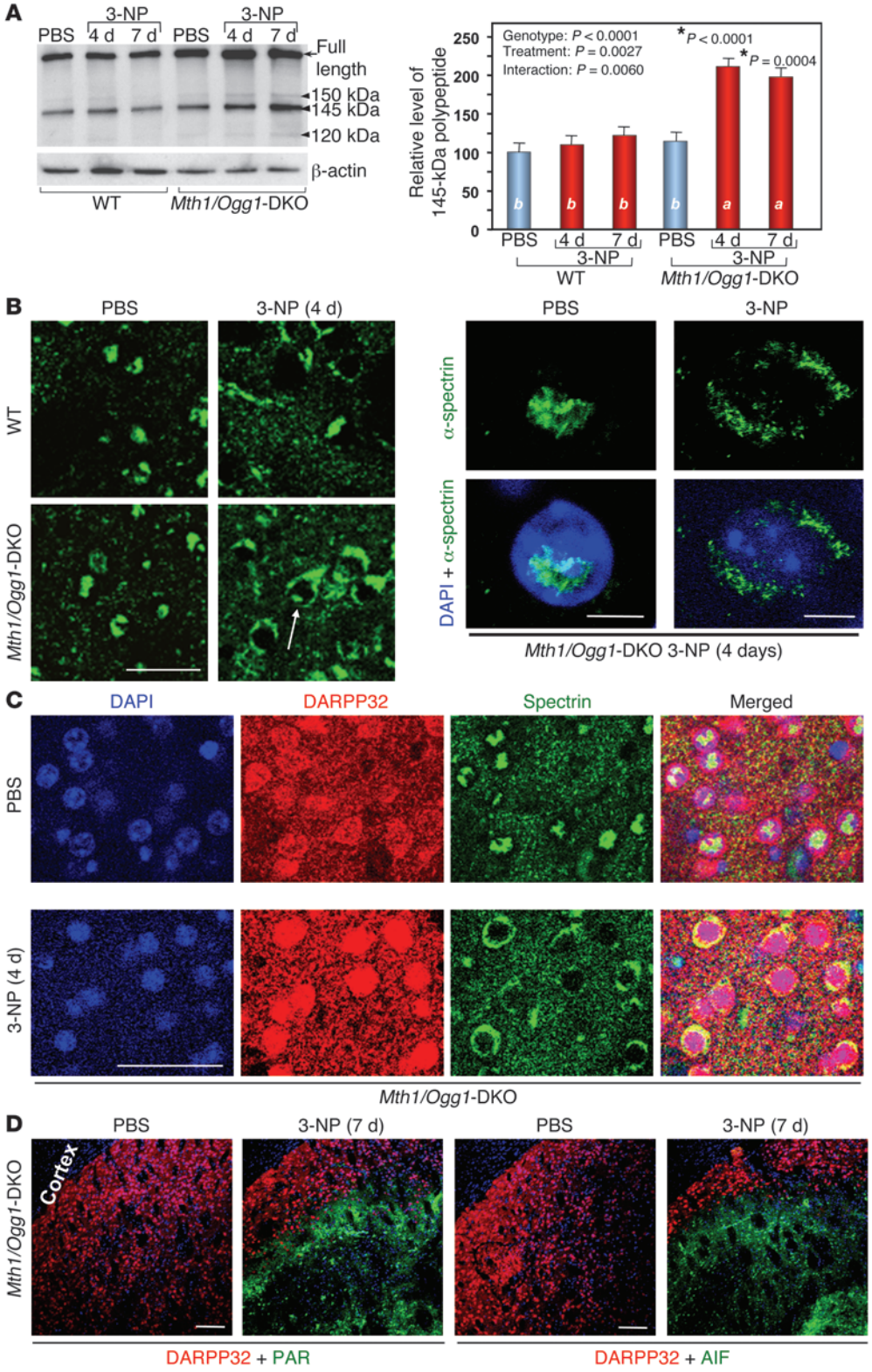

Figure 4
3-NP induces striatal degeneration dependent on calpain or PARP-AIF in *Mth1/Ogg1*-DKO mice. (**A**) Enhanced cleavage of α-spectrin by calpain in DKO striatum. Relative levels of the 145-kDa polypeptides are shown in the bar graph (right) (n = 3). Data are shown as LS means ± SEM. Levels not connected with the same letter are significantly different (Tukey's HSD test). *P, compared with the corresponding WT samples.(**B**) Altered localization of α-spectrin on the fourth day of 3-NP exposure in the DKO striatum. Localization of α-spectrin signal was changed after 3-NP exposure (arrow) (left). Scale bar: 50 μm. Magnified image showing the change of signal from nuclear to perinuclear localization (right). Scale bar: 5 μm. (**C**) Perinuclear localization of α-spectrin is evident in MSNs in the DKO striatum after 3-NP exposure. Scale bar: 25 μm. (**D**) Increased IRs for PAR and AIF in the DKO striatum where MSNs were largely depleted after 3-NP exposure. Scale bar: 50 μm.

IR was evident in DARPP32-positive neurons, while nuclear ssDNA IR was detected in F4/80-positive microglia (Figure 10, C and D) and cytoplasmic ssDNA IR was colocalized with TFAM IR after exposure to 3-NP for 7 days (Figure 10E). Moreover, we confirmed that cytoplasmic α-spectrin IRs and nuclear PAR IR were detected only in the *Ogg1*-KO but not the *Ogg1/Mutyh*-DKO striatum after exposure to 3-NP, as seen in *Mth1/Ogg1*-DKO mice (data not shown).

Finally, we confirmed that *Ogg1/Mutyh*-DKO mice exhibit resistance to 3-NP–induced locomotor dysfunction similar to that of *Mutyh*-KO mice (Supplemental Figure 7).

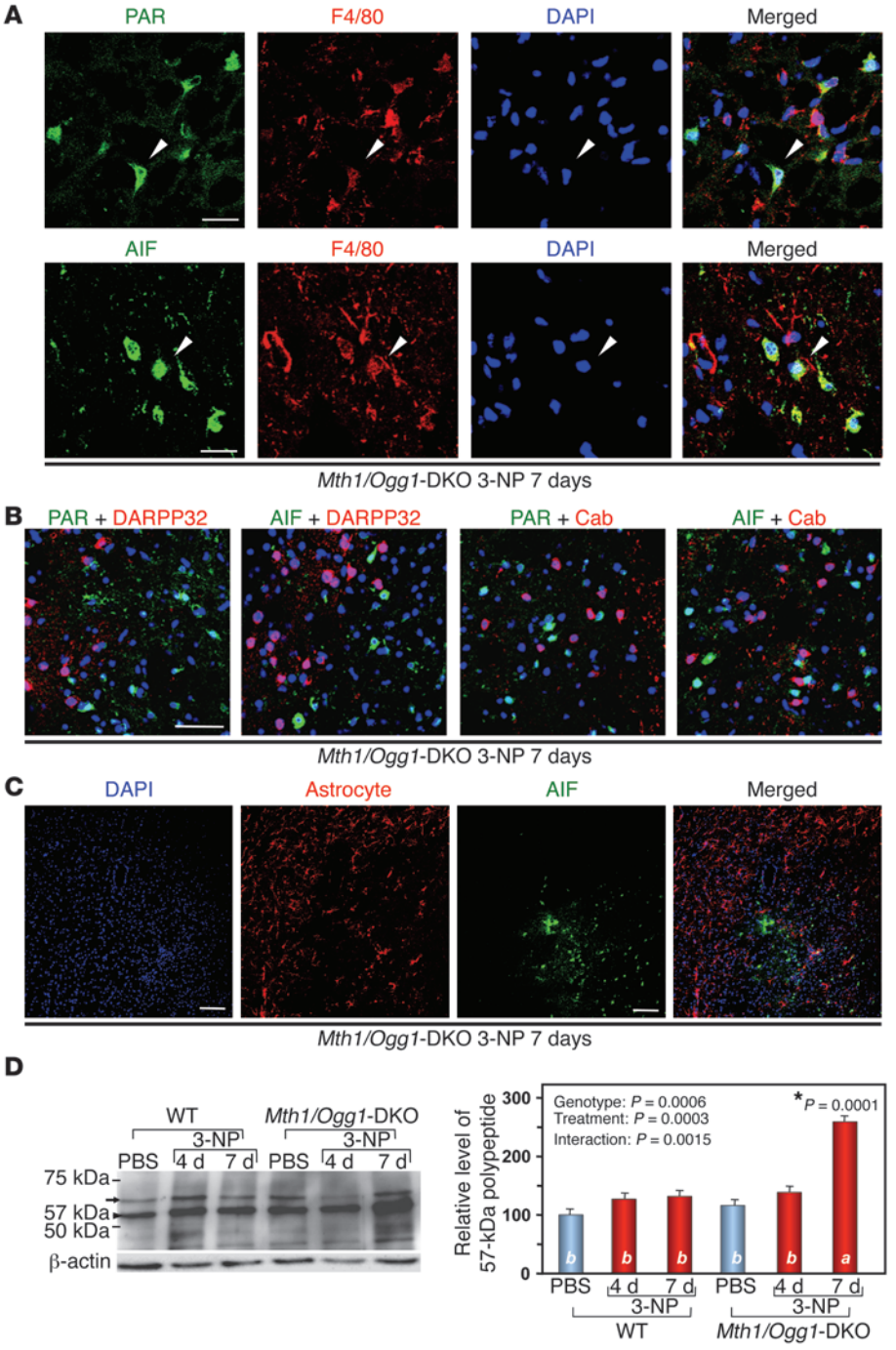

Figure 5
3-NP induces PAR and AIF accumulation in striatal microglia in *Mth1/Ogg1*-KDO mice. (**A**) Microglia in the DKO striatum exhibited IRs for PAR/AIF. Scale bars: 20 μm. (**B**) PAR and AIF were not accumulated in MSNs after 3-NP exposure. PAR/AIF, DARPP32 and calbindin (Cab), and DAPI were detected. Scale bar: 50 μm. (**C**) AIF was not accumulated in astrocytes. Scale bar: 50 μm. (**D**) 3-NP enhanced processing of AIF in DKO striatum. A 67-kDa mitochondrial form of AIF (arrow) and a 57-kDa nuclear form (arrowhead) are shown (left). Relative levels of the 57-kDa polypeptides are shown in a bar graph (right) ($n = 3$). In **D**, data are shown as LS means ± SEM. Levels not connected with the same letter are significantly different (Tukey's HSD test). **P*, compared with the corresponding WT samples.

Taken together, these results indicate that 3-NP–induced striatal degeneration is largely dependent on MUTYH function under conditions of OGG1 deficiency as well as MTH1/OGG1 deficiency.

Discussion

In the present study, we demonstrated that 8-oxoG accumulated within mtDNA and nDNA under conditions of oxidative stress is differentially involved in neurodegeneration through activation of the calpain and PARP/AIF pathways. MTH1 and OGG1, which prevent accumulation of 8-oxoG in the respective DNAs, protect the brain, while MUTYH, which initiates excision repair of adenine opposite 8-oxoG, triggers neurodegeneration.

We thus propose that the neurotoxicity of oxidative stress in the mammalian brain predominantly results from MUTYH-initiated excision repair of adenine opposite 8-oxoG, which is mostly derived from 8-oxo–dGTP accumulated in the nucleotide pool under oxidative stress.

MTH1 and OGG1 suppress neurodegeneration as well as mutagenesis and carcinogenesis by preventing accumulation of 8-oxoG in cellular DNAs. It has been widely accepted that both degenerative diseases and cancers are tightly associated with

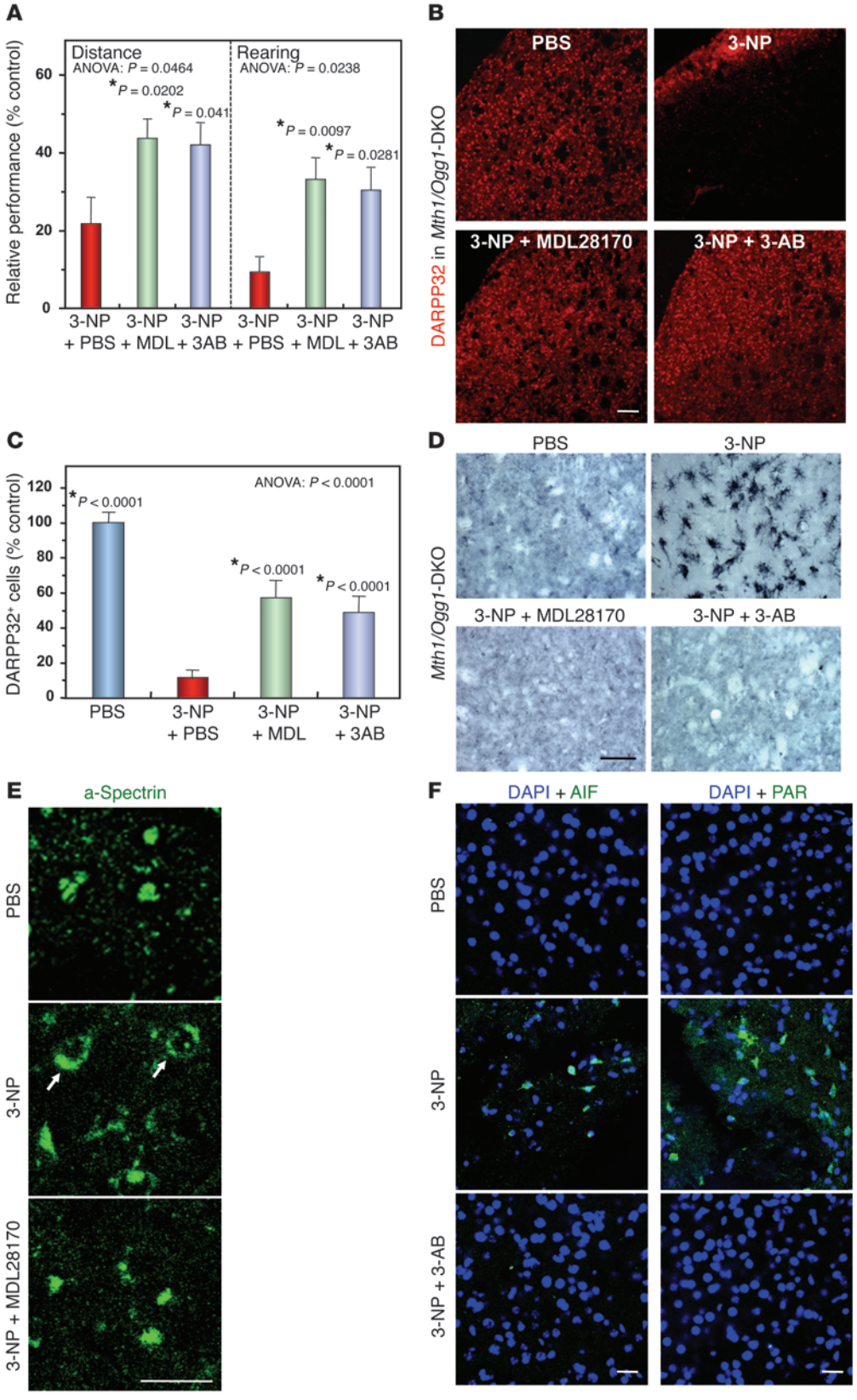

Figure 6
Calpain and PARP inhibitors suppress striatal degeneration and improve motor impairments in *Mth1*/*Ogg1*-DKO mice induced by 3-NP. (**A**) MDL-28170 (MDL), a cell-permeable calpain inhibitor, and 3-AB, an inhibitor of PARP, efficiently prevented 3-NP–induced motor impairments in DKO mice. Numbers of animals examined per condition are 7 (3-NP + PBS), 6 (3-NP + MDL), and 9 (3-NP + 3AB). (**B**) MDL or 3-AB suppressed loss of MSNs by 3-NP. DARPP32-positive cells (red) were detected. Scale bar: 50 μm. (**C**) MDL and 3-AB significantly suppressed loss of DARPP32-positive cells by 3-NP. Numbers of animals examined per condition are 4 (PBS), 4 (3-NP + PBS), 6 (3-NP + MDL), and 6 (3-NP + 3AB). Data are shown as LS means ± SEM. (**D**) MDL or 3-AB effectively diminished microgliosis. F4/80-positive cells (dark blue) were detected. Scale bar: 50 μm. (**E**) Calpain inhibitor inhibits perinuclear distribution of α-spectrin. Arrows, altered localization of α-spectrin. Scale bar: 50 μm. (**F**) The PARP inhibitor suppresses PAR/AIF. Scale bar: 50 μm. In **A** and **C**, the results of 1-way ANOVA are shown. **P*, compared with 3-NP + PBS (Hsu's MCB test).

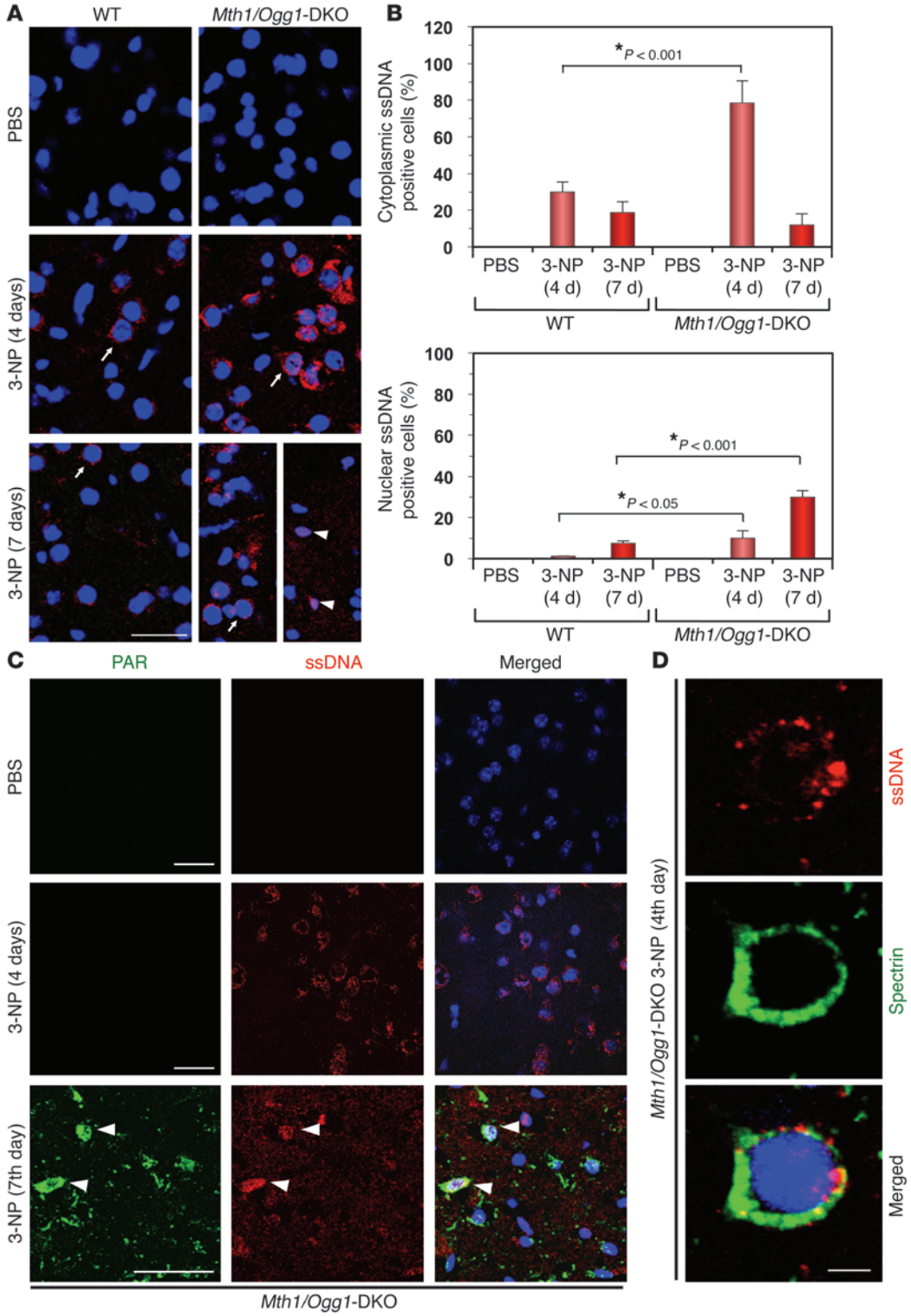

Figure 7
3-NP significantly increases accumulation of ssDNA with a delayed increase in poly(ADP-ribosyl)ation in the *Mth1*/*Ogg1*-DKO striatum. (**A**) Detection of ssDNA in striatum exposed to 3-NP. Strong cytoplasmic ssDNA IR was heavily detected in the *Mth1*/*Ogg1*-DKO striatum on the fourth day, whereas nuclear ssDNA IR was mostly seen in the DKO striatum on the seventh day, especially in the dorsolateral striatum where MSNs were lost. Arrows, cytoplasmic ssDNA+DAPI; arrow heads, nuclear ssDNA+DAPI. Scale bar: 50 μm. (**B**) The percentages of cells showing positive cytoplasmic and nuclear ssDNA IR in dorsolateral striatum were counted. The numbers of animals examined per condition are WT PBS ($n = 4$), 3-NP 4 days ($n = 4$), 3-NP 7 days ($n = 3$), DKO mice ($n = 4$) for each group. Data are shown as LS means ± SEM. (**C**) PAR IR detected in nuclear ssDNA-positive cells in DKO striatum on the seventh day of 3-NP exposure. Note that PAR IR was only detected on the seventh day, and was mostly colocalized with nuclear ssDNA IR (arrowheads). Scale bar: 50 μm. (**D**) Cytoplasmic ssDNA IR was detected in cytoplasmic α-spectrin–positive cells in DKO striatum after 3-NP exposure (fourth day). Scale bar: 5 μm.

DNA damage (1, 4). We previously showed that *Mth1*-KO and *Ogg1*-KO mice exhibit increased incidence of spontaneous tumors in liver and lung, respectively. This was accompanied by accumulation of 8-oxoG in their nDNAs, thus demonstrating that MTH1 and OGG1 prevent accumulation of 8-oxoG in nDNA, thereby suppressing mutagenesis and carcinogenesis (12, 13). However, we also found that mice lacking both MTH1 and OGG1 developed no lung tumors, although 8-oxoG was highly accumulated in nDNA (13). This observation suggests that excess accumulation of 8-oxoG under combined deficiency of MTH1 and OGG1 may induce tumor cell death, thereby leading to diminished occurrence of lung tumors (41). Furthermore,

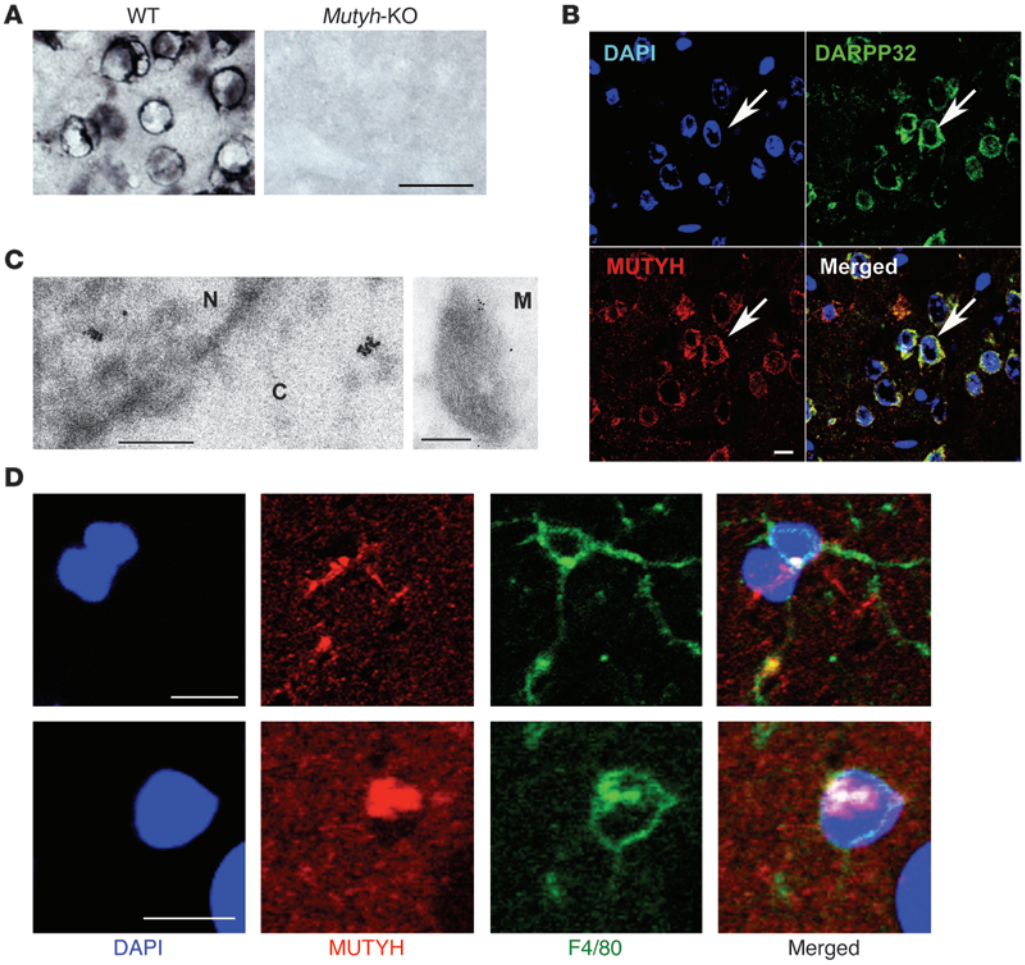
A
WT
Mutyh-KO
B
DAPI
DARPP32
MUTYH
Merged
C
N
C
M
D
DAPI
MUTYH
F4/80
Merged
E
Genotype: P = 0.0887
Treatment: P < 0.0001
Interaction: P = 0.0451
Rearing
Relative performance (%)
150
100
50
0
a
c
d
a
*P = 0.0081
b
d
PBS
120
150
PBS
120
150
3-NP (mg/kg/d)
3-NP (mg/kg/d)
WT
Mutyh-KO
F
PBS
3-NP
WT
Mutyh-KO
G
PBS
3-NP
WT
Mutyh-KO
Genotype: P = 0.0703
Treatment: P < 0.0001
Interaction: P = 0.1376
Cytochrome c oxidase activity (% control)
140
120
100
80
60
40
20
0
a
c
a
*P = 0.0228
b
PBS
3-NP
PBS
3-NP
WT
Mutyh-KO

Figure 8
Mutyh-KO mice are resistant to 3-NP–induced motor impairment and mitochondrial degeneration. (**A**) Expression of MUTYH in mouse striatum. MUTYH IRs were detected in WT but not *Mutyh*-KO brains. Scale bar: 25 μm. (**B**) MUTYH IRs were mostly detected in cytoplasm of DARPP32-positive cells in WT striatum. Scale bar: 10 μm. (**C**) Immunoelectron microscopy for MUTYH in WT striatum. C, cytoplasm; N, nucleus; M, mitochondrion. Scale bar: 250 nm. (**D**) MUTYH IR was detected in either cytoplasm or nuclei of F4/80-positive WT microglia. Scale bar: 10 μm. (**E**) Resistance of *Mutyh*-KO mice to 3-NP–induced motor impairment. *Mutyh*-KO mice exhibited a higher incidence of rearing in the open filed test after 3-NP exposure for 7 days than did WT mice. WT (PBS, $n = 6$; 3-NP 120 mg/kg/d, $n = 10$; 3-NP 150 mg/kg/d, $n = 10$); *Mutyh*-KO (PBS, $n = 7$; 3-NP 120 mg/kg/d, $n = 5$; 3-NP 150 mg/kg/d, $n = 10$). (**F**) Mitochondrial degeneration in striatum induced by 3-NP. Electron microscopy revealed disruption of outer and inner membranes (arrows) and cristae (arrowheads) in striatal mitochondria of WT but not *Mutyh*-KO mice (3-NP, 150 mg/kg/d, for 7 days). Scale bar: 200 nm. (**G**) Mitochondrial function was maintained in *Mutyh*-KO mice after 3-NP administration. Mitochondrial function was examined by histochemical detection of cytochrome oxidase activity. Images were obtained by DIC microscopy. WT (PBS, $n = 4$; 3-NP, $n = 4$); *Mutyh*-KO (PBS, $n = 5$; 3-NP, $n = 5$). Scale bar: 20 μm. In **E** and **G** (right), data are shown as LS means ± SEM. Levels not connected with the same letter are significantly different (Student's *t* test). **P*, compared with the corresponding WT sample.

we have shown that increased accumulation of 8-oxoG in nDNA and/or mtDNA causes cell death and that MTH1 and OGG1 suppress cell death (34, 40, 42).

We previously reported that *Mth1*-KO mice exhibit increased accumulation of 8-oxoG in the mtDNA of striatal nerve terminals of dopamine neurons after 1-methyl-4-phenyl-1,2,3,6-tetrahydropyridine administration, followed by more severe terminal degeneration of dopamine neurons in comparison to WT mice (31). MTH1 also efficiently suppresses the accumulation of 8-oxoG in mtDNA in the hippocampus caused by kainate-induced excitotoxicity, especially in microglia (43). Moreover, it has been shown that human MTH1 transgenic mice are resistant to 3-NP–induced striatal degeneration (27), suggesting that increased accumulation of 8-oxoG in brain causes neurodegeneration.

In the present study, we showed that double deficiency of MTH1 and OGG1 renders the striatum highly vulnerable to 3-NP–induced neurodegeneration, accompanied by highly increased accumulation of 8-oxoG in both the mtDNA of MSNs and the nDNA of microglia in the striatum. This is the first experimental evidence that OGG1 and MTH1 cooperatively suppress 8-oxoG accumulation in brain DNAs, thus protecting the brain from neuronal loss and microgliosis, which result in severe neurodegeneration and behavioral impairments.

Mitochondria prepared from caudate nucleus as well as other regions of mouse brain possess substantial levels of OGG1 incision activity (44). In the present study, we found that OGG1 was predominantly localized in the mitochondria of MSNs in normal striatum (Figure 1A) and that OGG1 deficiency significantly increased accumulation of mitochondrial 8-oxoG and ssDNA in MSNs after exposure to 3-NP. Considering these findings together, we concluded that mitochondrial OGG1 is crucial to protect striatal MSNs from oxidative stress.

MUTYH suppresses carcinogenesis but promotes neurodegeneration by inducing cell death. We have shown that *Mutyh*-KO mice exhibit the most significant increase in spontaneous occurrence of tumors among *Mth1*-, *Ogg1*-, and *Mutyh*-KO mice (14). It has been reported that *Ogg1*/*Mutyh*-DKO mice (15) and *Mth1*/*Ogg1*/*Mutyh*–triple-KO mice exhibit markedly increased spontaneous tumorigenesis in various tissues over a much shorter period (our unpublished observations). These observations indicate that MUTYH functions as the strongest suppressor of tumorigenesis among the 3, because *Mth1*/*Ogg1*-DKO mice develop no lung tumors whereas *Ogg1*-KO mice do (13). Thus, we hypothesized that MUTYH induces cell death, thereby suppressing tumorigenesis in the absence of MTH1 and OGG1. We previously showed that MUTYH is required for generation of SSBs in DNA and induction of cell death when 8-oxoG is highly accumulated in either nDNA or mtDNA under conditions of oxidative stress (34, 40, 41).

In the present study, we found that MUTYH protein is highly expressed in the striatum and is mostly present in the mitochondria of MSNs and that *Ogg1*/*Mutyh*-DKO mice exhibit markedly increased resistance to 3-NP–induced striatal degeneration in comparison with *Ogg1*-KO mice and even WT mice. These results clearly demonstrate that MUTYH enhances neurodegeneration through the induction of cell death once 8-oxoG becomes accumulated in neurons and/or microglia.

MUTYH-initiated BER induces accumulation of SSBs in DNA, thereby triggering 2 distinct cell death pathways dependent on calpain or PARP-AIF. We previously established that MUTYH initiates the 2 distinct pathways of cell death while 8-oxoG accumulates selectively in mtDNA or nDNA in *Ogg1*-KO cell lines (34). In the present study, we found that 8-oxoG is significantly accumulated first in the mtDNA of MSNs ($P < 0.0001$) and then in the nDNA of microglia during striatal degeneration caused by 3-NP in the absence of OGG1 and/or MTH1. This is followed by selective accumulation of SSBs in each type of DNA. Calpain activation was observed in MSNs, while nuclear accumulation of PAR-polymer and AIF was evident in microglia. Calpain activation, PARP-AIF activation, and accumulation of SSBs were observed in *Ogg1*-KO mice, but were efficiently suppressed by a lack of MUTYH, which initiated BER of adenines inserted opposite 8-oxoG (41). Moreover, administration of inhibitors of calpain or PARP to *Mth1*/*Ogg1*-DKO mice efficiently suppressed 3-NP–induced loss of MSNs and microgliosis in the striatum, and this was followed by improvement of motor impairment. Considering these observations together, we concluded that MUTYH-initiated BER induces accumulation of SSBs in DNA, thereby triggering 2 distinct cell death pathways dependent on calpain or PARP-AIF, as summarized in Figure 11. The anti-ssDNA antibody used in the present study also recognizes single-stranded regions of double-stranded breaks (DSBs) generated by resection of the ends (45). It is thus possible that DSBs may also be generated through incision of the template strand if there are other types of damaged bases close to 8-oxoG in the template DNA generated under increased oxidative stress.

Recently, Foti et al. reported that cytotoxicity of bactericidal antibiotics such as β-lactams and quinolones predominantly results from lethal double-strand DNA breaks caused by incomplete repair of closely spaced 8-oxoG lesions and is efficiently suppressed by *mutM*/*mutY*-double deficiency (5). Considered together with our previous findings (28, 34, 40–42), it is noteworthy that 8-oxoG accumulated in the genome causes cell death through a common mechanism from bacteria to mammals. In the mammalian brain, however, there are different types of cells, such as neurons and microglia, and each cell has 2 distinct genomes, 1 in the nucleus, and 1 in mitochondria. Our findings in the present study

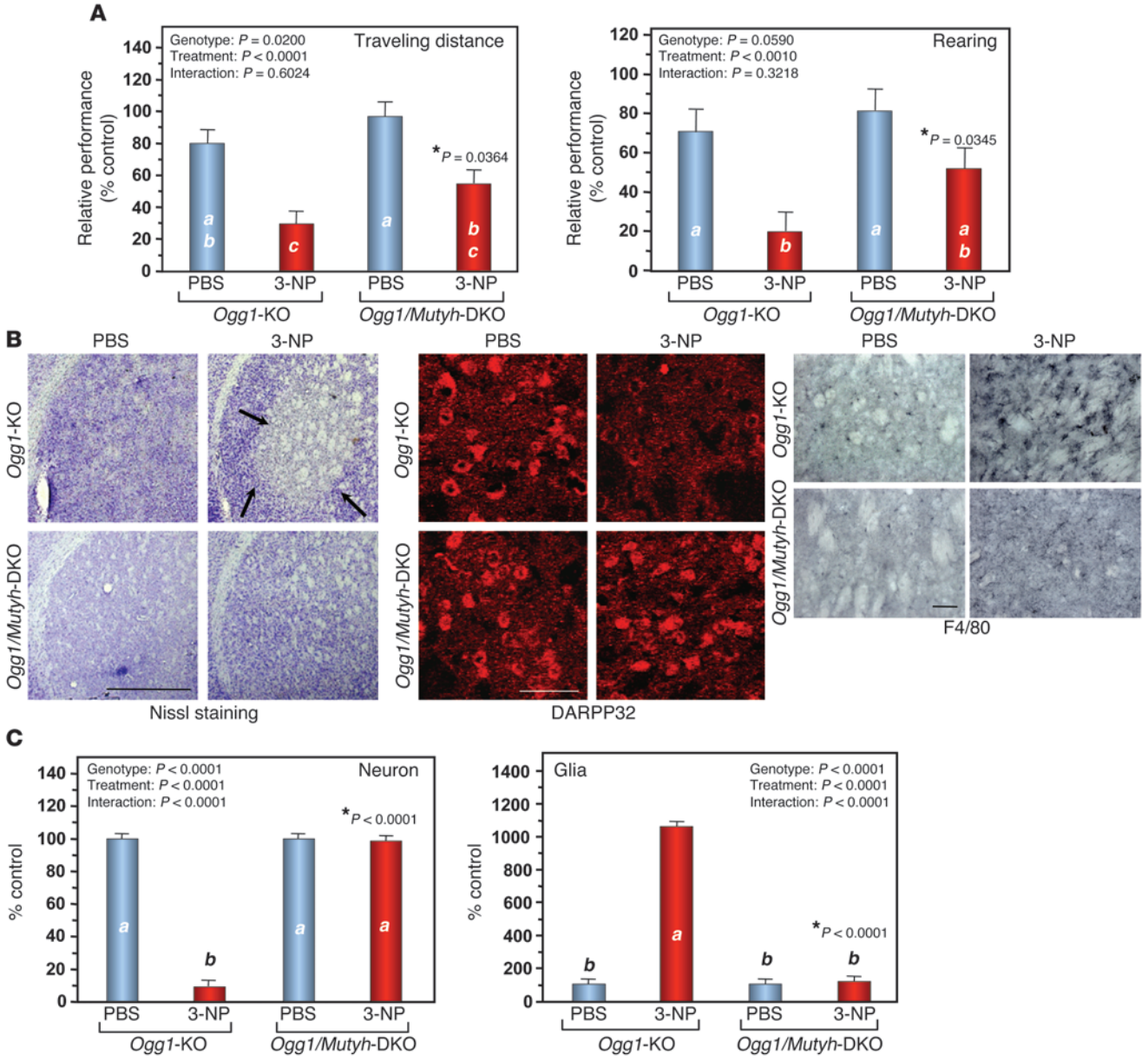

Figure 9

MUTYH deficiency ameliorates 3-NP–induced motor impairments and striatal degeneration in *Ogg1*-KO mice. (**A**) MUTYH deficiency ameliorates 3-NP–induced motor impairments in *Ogg1*-KO mice. *Ogg1*/*Mutyh*-DKO mice exhibited better performances in the open-field test after exposure to 3-NP for 7 days than did *Ogg1*-KO mice. *Ogg1*-KO (PBS, $n = 7$; 3-NP, $n = 8$); *Ogg1*/*Mutyh*-DKO (PBS, $n = 6$; 3-NP, $n = 7$). (**B**) MUTYH deficiency suppresses striatal degeneration. Nissl staining (left panels). DARPP32-positive MSNs (center panels). F4/80-positive microglia (3,3′-diaminobenzidine/nickel staining, right panels). Scale bar: 1 mm (left); 50 μm (center); 50 μm (right). (**C**) The numbers of neurons and glial cells in the dorsolateral striatum with or without 3-NP exposure for 7 days. Cells were counted in Nissl-stained sections, $n = 3$ for each group. Data are shown as LS means ± SEM. Levels not connected with the same letter are significantly different. *P, compared with *Ogg1*-KO mice exposed to 3-NP.

show for what we believe is the first time that neurodegeneration is a complex process caused by 8-oxoG accumulated in the 2 distinct genomes in the brain.

Neurodegeneration induced by 8-oxoG and MUTYH depends on both replication of mtDNA in neurons and nDNA in microglia. Overexpression of human MTH1 in mouse striatum efficiently abrogates 3-NP–induced striatal degeneration accompanied by effective suppression of 8-oxoG accumulation in the striatum (27). *Mth1*/*Ogg1*-DKO mice exhibited the highest susceptibility to 3-NP–induced striatal degeneration with the highest levels of 8-oxoG in striatal DNAs. These findings indicate that the major source of 8-oxoG accumulated in DNA are 8-oxo-dGTP generated in nucleotide pool; the former is repaired by OGG1 and the latter is hydrolyzed by MTH1.

DNA replication is essential for accumulation of 8-oxoG in the respective DNA; moreover, insertion of adenine opposite 8-oxoG also depends on replication. Neurons are postmitotic and only mtDNA but not nDNA is always replicated in neurons in order

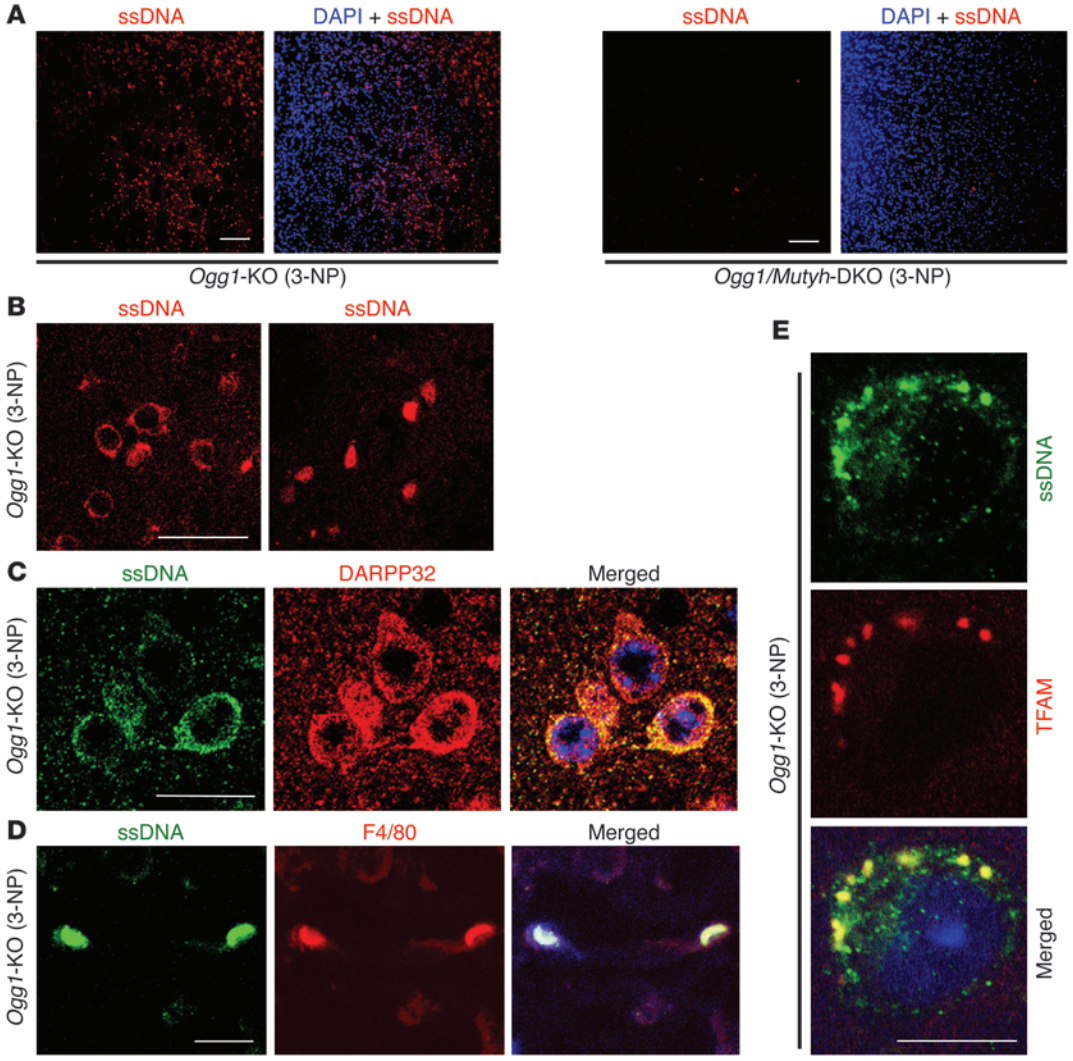

Figure 10
MUTYH deficiency suppresses both nuclear and mitochondrial ssDNA accumulation in *Ogg1*-KO mice. (**A**) ssDNA accumulation was only found in *Ogg1*-KO mice after exposure to 3-NP for 7 days. Scale bar: 50 μm. (**B**) Nuclear and cytoplasmic ssDNA were detected in *Ogg1*-KO mice after exposure to 3-NP for 7 days. Scale bar: 50 μm. (**C**) Cytoplasmic ssDNA IR was specifically detected in *Ogg1*-KO MSNs after exposure to 3-NP for 7 days. Scale bar: 20 μm. (**D**) Nuclear ssDNA IR was specifically detected in *Ogg1*-KO microglia after exposure to 3-NP for 7 days. Scale bar: 20 μm. (**E**) Cytoplasmic ssDNA IR was colocalized with TFAM IR in *Ogg1*-KO striatum after exposure to 3-NP for 7 days. Scale bar: 10 μm.

to provide the energy essential for maintenance of neuronal functions. 8-oxoG is therefore dominantly accumulated in mtDNA of neurons under conditions of oxidative stress, resulting in SSB accumulation in mtDNA during MUTYH-initiated BER of adenine inserted opposite 8-oxoG. In contrast, microglia are mitotic; thus, 8-oxoG and SSBs accumulated in nDNA dependent on their replication and MUTYH-initiated BER (Figure 11). Thus, replication of the respective DNAs in neurons and microglia determines which of the 2 separate signaling pathways must be activated upon accumulation of 8-oxoG under conditions of oxidative stress.

Microgliosis is a delayed event in striatal degeneration induced by 3-NP (Figure 1D); therefore, it is likely that accumulation of 8-oxoG followed by ssDNA accumulation in nDNA of microglia (Figures 3H and 7B) is not due to a direct effect of mitochondrial ROS generated in MSNs immediately after exposure to 3-NP. Neurons damaged by mitochondrial ROS thereafter induce a delayed inflammatory response, resulting in microgliosis, which is known to be accompanied by secondary generation of ROS in brain (46). Since inhibition of PARP activity, which is activated by SSBs accumulated in the nDNA of microglia resulting in AIF activation (Figure 5, A and D), efficiently suppressed neuronal loss as well as microgliosis, ROS generated in microglia may in turn attack neurons to promote the degenerative process as suggested by Brouillet et al. (36), thus initiating a vicious cycle of neurodegeneration.

Growing evidence suggests that mitochondrial dysfunction is generally associated with neurodegenerative diseases (47) and that microglial activation is also involved in the pathogenesis of most forms of neurodegeneration (48). It is known that activation of calpain, PARP, and AIF is involved in various neurodegenera-

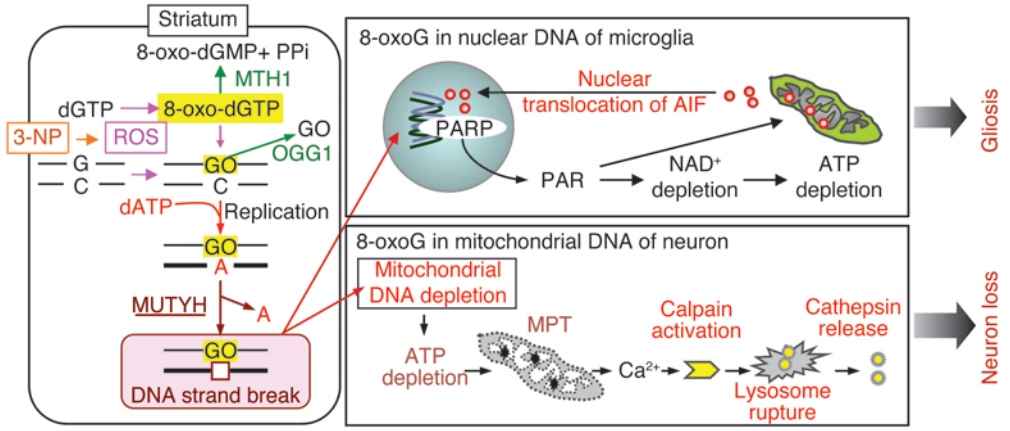

Figure 11

Molecular mechanisms underlying 8-oxoG–induced striatal degeneration. Chronic administration of the mitochondrial neurotoxin 3-NP to mutant mice lacking OGG1, which excises a major oxidative base lesion 8-oxoG (GO) opposite cytosine from DNA, and/or MTH1, which hydrolyses 8-oxo–dGTP in the nucleotide pool to prevent its harmful incorporation into DNA, causes significantly increased accumulation of 8-oxoG in the striatum. At an early stage, buildup of 8-oxoG in the mitochondrial DNA of striatal MSNs causes calpain-dependent neuronal loss triggered by mitochondrial MUTYH-initiated BER of adenines opposite 8-oxoG. In the later stages, buildup of 8-oxoG in the nuclear DNA of microglia causes PARP-dependent nuclear translocation of mitochondrial AIF triggered by nuclear MUTYH-initiated BER, thus resulting in microgliosis. Two distinct pathways of cell death, both dependent on MUTYH-initiated BER (34), result in severe striatal degeneration and motor impairments.

tive diseases such as AD, PD, and HD (38, 49), in which 8-oxoG is a common molecular marker (50), together with altered expression of MTH1, OGG1, and MUTYH (16, 19–22). Inhibition of calpain and PARP has been considered to be a potential therapeutic approach for neurologic disorders (38, 49).

Our findings in the present study show that 2 distinct molecular pathways are separately activated in the mitochondria of neurons and the nuclei of microglia through oxidative DNA damage and its repair, thus providing insights into the molecular mechanisms underlying neurodegeneration under conditions of oxidative stress as well as providing therapeutic targets for neurodegenerative diseases. Suppression of MUTYH may thus be an efficient strategy for protecting the brain under conditions of oxidative stress. However, it will be important not to increase the risk of carcinogenesis under MUTYH suppression; therefore, further experimental evaluation is essential.

Methods

Mice. We previously established *Mth1*, *Ogg1*, and *Mutyh* gene KO mice (12, 13, 51). Heterozygous mice (*Mth1*$^{+/-}$, *Ogg1*$^{+/-}$, *Mutyh*$^{+/-}$) were backcrossed to C57BL/6J mice (Clea Japan) for more than 15 generations, thereby ensuring the mice were on a pure C57BL/6J genetic background. Homozygous KO mice (*Mth1*$^{-/-}$, *Ogg1*$^{-/-}$, *Mutyh*$^{-/-}$) were generated by crossing of the corresponding heterozygous mice and inbred for 2 to 3 generations to obtain the mice used in each experiment. *Mth1*$^{+/-}$*Ogg1*$^{+/-}$ double-heterozygous mice obtained by crossing of *Mth1*$^{+/-}$ and *Ogg1*$^{+/-}$ mice were crossed to obtain *Mth1*$^{-/-}$*Ogg1*$^{-/-}$ (*Mth1*/*Ogg1*-DKO) mice and were inbred for 2 to 3 generations to obtain the mice used in each experiment. *Ogg1*$^{+/-}$*Mutyh*$^{+/-}$ double-heterozygous mice were obtained by crossing *Ogg1*$^{+/-}$ and *Mutyh*$^{+/-}$ mice to obtain *Ogg1*$^{-/-}$*Mutyh*$^{-/-}$ (*Ogg1*/*Mutyh*-DKO), and these were inbred for 2 to 3 generations to obtain the mice used in each experiment. C57BL/6J mice were used as the WT strain. All animals were maintained in an air-conditioned, specific pathogen–free room with time-controlled lighting.

Treatment with 3-NP. Ten-week-old male mice were used. 3-NP (Sigma-Aldrich) was dissolved in PBS and systemically administered via an i.p. implanted osmotic minipump (1007D, Alzet; delivering 0.5 μl/h for 7 days). All animals were subjected to surgical operations between 9:00 am and 12:00 pm. Mice were anesthetized with pentobarbital (30 mg/kg, i.p.), an incision was made in the abdomen, and the osmotic minipump was implanted into the i.p. cavity. In typical experiments, mice were exposed to 120 mg of 3-NP/kg/d for 7 days, and the control mice were subjected to implantation of the osmotic minipump containing PBS for 7 days. To compare 3-NP resistance between *Mutyh*-KO and WT mice, a higher dose of 3-NP (150 mg/kg/d) was applied.

Treatment with MDL28170 and 3-AB. A calpain inhibitor (MDL28170, Biomol) or a poly-(ADP-ribose) polymerase inhibitor (3-AB; Sigma-Aldrich) was administered together with 3-NP to *Mth1*/*Ogg1*-DKO mice. Two osmotic minipumps prefilled with 3-NP (120 mg/kg/d) and MDL28170 (50 mg/kg/d, dissolved in dimethyl sulfoxide, then diluted in PBS) or 3-AB (30 mg/kg/d, dissolved in PBS) were simultaneously implanted for 7 days. Control mice were implanted with 2 minipumps prefilled with 3-NP (120 mg/kg/d) and PBS.

Behavioral analysis. 3-NP–induced motor symptoms were evaluated using a quantitative neurological scale based on previous reports (29, 30). Neurological scores were defined as follows: score = 0, normal behavior; 1, general slowness of displacement resulting from mild hind limb impairment; 2, incoordination and marked gait abnormality; 3, hind limb paralysis; 4, incapacity to move resulting from forelimb and hind limb impairment; 5, recumbency.

Spontaneous locomotor activity in the home cage was measured using a digital counter with an infrared beam sensor (NS-ASS01; Neuroscience, Inc.), placed about 200 mm above the center of the home cage (27 × 14 × 15 cm), and analyzed using DAS-008 software.

To evaluate the extent of motor impairment induced by 3-NP exposure, an open-field test was performed. Behavioral analysis was performed between 9:00 am and 12:00 pm. A mouse was placed in the center of a circular open field (60 cm in diameter, 30 cm deep). Motor activity was quantified using an automated video tracking system, the video-image motion analyzer AXIS-90 (Neuroscience Inc.). Traveling distance and numbers of rearing behaviors were measured for 5 minutes. To avoid a reduction in motor activity due to habituation to the open field, motor activity was recorded only twice, on the day before implantation of the osmotic minipump (baseline performance) and on the seventh day after the operation. The number of animals examined is shown in each figure legend. Relative performance indicates the traveling distance or number of rearing times obtained on the seventh day after implantation of an osmotic minipump as a percentage of that obtained on the day before implantation.

Rotarod testing was performed between 9:00 am and 12:00 pm. The test was performed using an accelerating rotarod for mice (Model 7650; UGO Basile). Prior to 3-NP treatment, all mice were given 3 trials on the rotarod,

which was accelerated from 4 to 40 rpm over a 300-second period and kept at the top speed for more than 100 seconds each day for 3 consecutive days. On the third day, latency to fall from the rotarod was measured as a baseline performance. On the seventh day after implantation of the minipump, mice were tested on the rotarod, and latency to fall off was measured after 3-NP treatment.

Antibodies. The primary antibodies used were mouse monoclonal anti-8-oxo–dG (N45.1, JaICa, Fukuroi); rabbit anti-DARPP32 (Cell Signaling Technology); mouse anti-DARPP32 (BD Transduction Laboratories); rat anti-F4/80 (Oxford); goat anti-TFAM (Santa Cruz Biotechnology Inc.); mouse anti–α–spectrin (Chemicon); mouse anti-AIF (Santa Cruz Biotechnology Inc.); mouse anti-PAR (Trevigen), rabbit anti-ssDNA (Immuno-Biological Laboratories), rabbit anti-calbindin D-28K (Chemicon); rabbit anti-GFAP (Dako); rabbit anti-Hsp60 (Abcam); rabbit anti-OGG1, which recognizes the conserved region of human OGG1 proteins (52); rabbit anti-MTH1 (NB100-109, Novus Biologicals); and rabbit anti-MUTYH, which was raised against recombinant human MUTYH (53). The ssDNA antibody recognizes single-stranded regions of DNA with a length of at least 6 deoxynucleotides, which can be generated by SSBs or DSBs with resection of the ends (45, 54).

Immunohistochemistry. Tissue preparation and immunohistochemical analyses were performed as described previously (31). Brains were cut on a cryostat at a thickness of 40 μm and collected as free-floating sections in PBS; these were then processed immediately for immunohistochemistry (IHC). Free-floating sections were subjected to appropriate pretreatment and reaction with a primary antibody and then processed using a Vector ABC kit (Vector Laboratories) with the proper biotinylated secondary antibody. Then, the 3,3′-diaminobenzidine (DAB)/nickel (Vector Laboratories) reaction was used to visualize the bound secondary antibody. Some sections were counterstained with cresyl violet. Digital images were acquired using an Axioskop2 Plus microscope, equipped with an AxioCam CCD camera, and Axiovision 3.1 imaging software (Carl Zeiss Inc.) was used.

Laser-scanning confocal immunofluorescent microscopy. Free-floating sections incubated with the appropriate primary antibody were then further incubated with a proper Alexa Fluor–labeled secondary antibody (Invitrogen) in a solution containing DAPI (0.05 μg/ml, Sigma-Aldrich). Confocal images were acquired using a confocal laser microscopy system (LSM 510META-V3.2 software; Carl Zeiss Inc.) attached to an inverted microscope (Axiovert 200M). Images of the immunostained sections were taken within 48 hours.

Quantitative immunodetection of 8-oxoG. For immunodetection of 8-oxoG in nDNA or mtDNA, free-floating sections were pretreated as described previously (31, 32). Briefly, to detect 8-oxoG in the mtDNA, sections were pretreated only with RNase (5 mg/ml; Sigma-Aldrich) and were directly subjected to IHC with the anti-8-oxo–dG antibody. To detect 8-oxoG in nDNA, RNase-treated sections were further pretreated with 2N HCl to denature the nDNA, thus enabling the antibody to access 8-oxoG in nDNA. These pretreated sections were subjected to IHC with the anti–8-oxo–dG antibody. The intensity of 8-oxoG IR in the whole striatum was measured in each digital image using ImageJ 1.42 (NIH). Pretreated sections reacted with the anti–8-oxo–dG as described above were also subjected to immunofluorescence microscopy with a proper Alexa Fluor–labeled secondary antibody. The mitochondrial 8-oxo–dG index in a single neuron was measured in each laser confocal image of the immunofluorescence samples using ImageJ. Twenty neurons were measured to obtain the mean mitochondrial 8-oxo–dG index for each animal.

Quantification of the level of nuclear 8-oxo–dG in striatum by LC-MS/MS. Ten-week-old male WT and *Mth1/Ogg1*-DKO were subjected to PBS or 3-NP administration. The mice were euthanized by cervical dislocation, and the striata were immediately removed and frozen in liquid nitrogen. The tissues were stored at –80°C and analyzed within 7 days of collection. No difference in the level of 8-oxo–dG was observed between tissues stored at –80°C and freshly isolated tissues. DNA was extracted from striata using the DNA Extractor TIS Kit (No. 296-67701, Wako) as described in the instructions for the kit, with a few modifications: 10 mM 2, 2, 6, 6-tetramethylpiperidine-N-oxyl (TEMPO, Wako) and 100 μM 2′-deoxycoformycin, an adenosine deaminase inhibitor provided by the Chemo-Sero-Therapeutic Research Institute (Kumamoto, Japan), were added to all reagents at all stages of manipulation. To allow for accurate quantitation of 8-oxo–dG and to account for the signal variability of the mass spectrometer, [^{15}N5]-labeled 8-oxo–dG (NLM-6715-0, Cambridge Isotope Laboratories Inc.) was added as a stable isotope internal standard prior to enzymatic hydrolysis of the DNA samples. The stable internal standards [^{15}N5] 8-oxo–dG, sodium acetate buffer (ABI, #400884, pH 4.5), nuclease P1 (Yamas), and acid phosphatase (P-0157; Sigma-Aldrich) were added to the DNA samples; samples were then transferred to filter tubes (Ultrafree-MC probind 0.45 μm; Millipore), and centrifuged at 12,000 *g* for 3 minutes. The digested samples were subjected to LC-MS/MS analysis using a Shimadzu VP-10 HPLC system connected to an API3000 MS/MS system (PE-SCIEX), and the ratios of 8-oxo–dG to 10^6 dG in the samples were determined as described previously (55).

Histochemical detection of mitochondrial cytochrome c oxidase activity. For detection of mitochondrial cytochrome *c* oxidase activity in frozen sections, brain sections (thickness, 40 μm) were prepared from WT and *Mutyh*-KO mice administered PBS or 3-NP (150 mg/kg/d) for 7 days. Brain sections were incubated for 3 hours at 37°C in a solution containing cytochrome *c* (0.3 mg/ml), DAB (0.5 mg/ml), and sucrose (40 mg/ml) in PBS. Then sections washed in PBS were dehydrated with ethanol, immersed in xylene and mounted on slide glass, and digital images were acquired. The intensity of DAB staining cytochrome *c* oxidase activity in the whole striatum was measured in each digital image using ImageJ 1.42.

Morphometric analysis. The densities of neurons and glial cells in the dorsolateral striatum (bregma, 0.86 mm to approximately 0.62 mm) (56) were estimated by counting those on cresyl violet–stained sections. Neurons were identified as large cells with typical morphological features including a round, oval, or polygonal shape, and glial cells were identified as cells with profiles distinguished by their small, round, and hyperchromatic nuclei. The density of MSNs in the dorsolateral striatum was estimated by counting DARPP32-positive cells.

Western blot analysis. Striata were isolated from *Mth1/Ogg1*-DKO or WT mice on the fourth and seventh days of exposure to 3-NP or on the seventh day of exposure to PBS. Mouse striata were homogenized in ice-cold lysis buffer containing 50 mM Tris-HCl, pH 8.0, 150 mM NaCl, 1.0% NP-40, 0.5% sodium deoxycholate, 0.1% SDS, and protease inhibitor mixture (Nacalai Tesque). The homogenates were then centrifuged at 89,000 *g* for 30 minutes at 4°C, and the supernatants were collected. Western blot analysis was performed according to previously described methods (57, 58). Protein concentration in the supernatant was measured using a DC protein assay kit (Bio-Rad). Equal amounts of total protein (5 μg) were separated by SDS-PAGE. Anti–α-spectrin (1:10,000), anti-AIF (1:500), and anti–β-actin (1:10,000) antibodies were used. The intensity of each band was quantified using an LAS1000 image analyzer and Image Gauge, version 3.2 software (Fujifilm).

Electron microscopy. For transmission electron microscopy, mouse brains were prefixed with 4% paraformaldehyde and 2.5% glutaraldehyde (TAAB Laboratories), washed with a cacodylate buffer, postfixed in osmium tetroxide (Nacalai Tesque), dehydrated in ascending concentrations of alcohol and uranyl acetate (MERCK), and embedded in epoxy resin (TAAB 812 resin. TAAB Laboratories). Ultrathin sections (100 nm) were cut, and examined under a transmission electron microscope (Tecnai 20; FEI Corp.). For electron microscopic immunocytochemistry to detect MUTYH

protein, fixed mouse brains were incubated in 2.3 M sucrose and then in 20% polyvinylpyrrolidone (Nacalai Tesque) prepared in 1.8 M sucrose. Ultrathin sections (100 nm) were cut, blocked in 3% BSA, incubated with rabbit anti-MUTYH antibody, then with a secondary antibody, anti-rabbit IgG-gold (10 nm; EY Lab.). Sections were post-fixed with 2.5% glutaraldehyde in 0.1 M cacodylate buffer, mounted with 0.1% uranyl acetate in 2% polyvinyl alcohol (Sigma-Aldrich), and examined under transmission electron microscope.

Statistics. Statistical analyses were conducted using JMP 9.02 (SAS Institute Inc.). Data are presented as least square (LS) means ± SEM. To assess statistical significance, we performed 1-way ANOVA for effects of treatment or 2-way ANOVA with interaction for effects of genotype and treatment, and interactions between genotype and treatment; results obtained by standard LS fits are shown. For multiple comparison tests, 1-way ANOVA analyses were followed by a post hoc Hsu's MCB test, while 2-way ANOVA analyses were followed by a post hoc Tukey's HSD test. Student's *t* test was applied for individual pairwise comparisons in all cases. The threshold for statistical significance was $P < 0.05$.

Study approval. The handling and killing of all animals were done in accordance with national prescribed guidelines, and ethical approval for the studies was granted by the Animal Care and Use Committee of Kyushu University.

Acknowledgments

This work was supported by grants from the Ministry of Education, Culture, Sports, Science and Technology of Japan (20013034), the Japan Society for the Promotion of Science (18300124, 19390114, 22221004, 22501014), and the Kyushu University Global COE program (Cell-rate Decision Function and Dysfunction in Homeostasis). We thank Yasunari Sakai, Dongchon Kang, Mami Noda, and Mizuki Ohno for helpful discussions; Ryo Ugawa (Laboratory for Technical Support, Medical Institute of Bioregulation, Kyushu University, Kyushu, Japan) for electron microscopy; and Setsuko Kitamura, Noami Adachi, Kazumi Asakawa, and Kaoru Nakabeppu for their technical assistance.

Received for publication May 29, 2012, and accepted in revised form September 13, 2012.

Address correspondence to: Yusaku Nakabeppu, Kyushu University, Division of Neurofunctional Genomics, Department of Immunobiology and Neuroscience, Medical Institute of Bioregulation, Kyushu University, 3-1-1 Maidashi, Higashi-ku, Fukuoka, 812-8582, Japan. Phone: 81.92.642.6800; Fax: 81.92.642.6791; E-mail: yusaku@bioreg.kyushu-u.ac.jp.

1. Ames BN, Shigenaga MK, Hagen TM. Oxidants, antioxidants, and the degenerative diseases of aging. *Proc Natl Acad Sci U S A*. 1993;90(17):7915–7922.
2. Finkel T, Holbrook NJ. Oxidants, oxidative stress and the biology of ageing. *Nature*. 2000; 408(6809):239–247.
3. Maynard S, Schurman SH, Harboe C, de Souza-Pinto NC, Bohr VA. Base excision repair of oxidative DNA damage and association with cancer and aging. *Carcinogenesis*. 2009;30(1):2–10.
4. Nakabeppu Y, Sakumi K, Sakamoto K, Tsuchimoto D, Tsuzuki T, Nakatsu Y. Mutagenesis and carcinogenesis caused by the oxidation of nucleic acids. *Biol Chem*. 2006;387(4):373–379.
5. Foti JJ, Devadoss B, Winkler JA, Collins JJ, Walker GC. Oxidation of the guanine nucleotide pool underlies cell death by bactericidal antibiotics. *Science*. 2012;336(6079):315–319.
6. Kasai H. Chemistry-based studies on oxidative DNA damage: formation, repair, and mutagenesis. *Free Radic Biol Med*. 2002;33(4):450–456.
7. Kasai H, Nishimura S. Hydroxylation of deoxyguanosine at the C-8 position by ascorbic acid and other reducing agents. *Nucleic Acids Res*. 1984; 12(4):2137–2145.
8. Sakumi K, et al. Cloning and expression of cDNA for a human enzyme that hydrolyzes 8-oxo-dGTP, a mutagenic substrate for DNA synthesis. *J Biol Chem*. 1993;268(31):23524–23530.
9. Furuichi M, et al. Genomic structure and chromosome location of the human mutT homologue gene *MTH1* encoding 8-oxo-dGTPase for prevention of A:T to C:G transversion. *Genomics*. 1994; 24(3):485–490.
10. Aburatani H, et al. Cloning and characterization of mammalian 8-hydroxyguanine-specific DNA glycosylase/apurinic, apyrimidinic lyase, a functional mutM homologue. *Cancer Res*. 1997; 57(11):2151–2156.
11. Slupska MM, Baikalov C, Luther WM, Chiang JH, Wei YF, Miller JH. Cloning and sequencing a human homolog (*hMYH*) of the *Escherichia coli mutY* gene whose function is required for the repair of oxidative DNA damage. *J Bacteriol*. 1996; 178(13):3885–3892.
12. Tsuzuki T, et al. Spontaneous tumorigenesis in mice defective in the *MTH1* gene encoding 8-oxo-dGTPase. *Proc Natl Acad Sci U S A*. 2001; 98(20):11456–11461.
13. Sakumi K, et al. *Ogg1* knockout-associated lung tumorigenesis and its suppression by Mth1 gene disruption. *Cancer Res*. 2003;63(5):902–905.
14. Sakamoto K, et al. MUTYH-null mice are susceptible to spontaneous and oxidative stress induced intestinal tumorigenesis. *Cancer Res.* 2007; 67(14):6599–6604.
15. Xie Y, et al. Deficiencies in mouse *Myh* and *Ogg1* result in tumor predisposition and G to T mutations in codon 12 of the *K-ras* oncogene in lung tumors. *Cancer Res*. 2004;64(9):3096–3102.
16. Shimura-Miura H, Hattori N, Kang D, Miyako K, Nakabeppu Y, Mizuno Y. Increased 8-oxo-dGTPase in the mitochondria of substantia nigral neurons in Parkinson's disease. *Ann Neurol*. 1999;46(6):920–924.
17. Wang J, Xiong S, Xie C, Markesbery WR, Lovell MA. Increased oxidative damage in nuclear and mitochondrial DNA in Alzheimer's disease. *J Neurochem*. 2005;93(4):953–962.
18. Polidori MC, Mecocci P, Browne SE, Senin U, Beal MF. Oxidative damage to mitochondrial DNA in Huntington's disease parietal cortex. *Neurosci Lett*. 1999;272(1):53–56.
19. Fukae J, et al. Expression of 8-oxoguanine DNA glycosylase (OGG1) in Parkinson's disease and related neurodegenerative disorders. *Acta Neuropathol*. 2005; 109(3):256–262.
20. Furuta A, Iida T, Nakabeppu Y, Iwaki T. Expression of hMTH1 in the hippocampi of control and Alzheimer's disease. *Neuroreport*. 2001;12(13):2895–2899.
21. Arai T, et al. Up-regulation of hMUTYH, a DNA repair enzyme, in the mitochondria of substantia nigra in Parkinson's disease. *Acta Neuropathol*. 2006; 112(2):139–145.
22. Iida T, Furuta A, Nishioka K, Nakabeppu Y, Iwaki T. Expression of 8-oxoguanine DNA glycosylase is reduced and associated with neurofibrillary tangles in Alzheimer's disease brain. *Acta Neuropathol*. 2002; 103(1):20–25.
23. Parent A. Extrinsic connections of the basal ganglia. *Trends Neurosci*. 1990;13(7):254–258.
24. Gould DH, Gustine DL. Basal ganglia degeneration, myelin alterations, and enzyme inhibition induced in mice by the plant toxin 3-nitropropanoic acid. *Neuropathol Appl Neurobiol*. 1982;8(5):377–393.
25. Brouillet E, et al. Chronic mitochondrial energy impairment produces selective striatal degeneration and abnormal choreiform movements in primates. *Proc Natl Acad Sci U S A*. 1995;92(15):7105–7109.
26. Brouillet E, Conde F, Beal MF, Hantraye P. Replicating Huntington's disease phenotype in experimental animals. *Prog Neurobiol*. 1999;59(5):427–468.
27. De Luca G, et al. A role for oxidized DNA precursors in Huntington's disease-like striatal neurodegeneration. *PLoS Genet*. 2008;4(11):e1000266.
28. Nakabeppu Y, Oka S, Sheng Z, Tsuchimoto D, Sakumi K. Programmed cell death triggered by nucleotide pool damage and its prevention by MutT homolog-1 (MTH1) with oxidized purine nucleoside triphosphatase. *Mutat Res*. 2010; 703(1):51–58.
29. Guyot MC, Hantraye P, Dolan R, Palfi S, Maziere M, Brouillet E. Quantifiable bradykinesia, gait abnormalities and Huntington's disease-like striatal lesions in rats chronically treated with 3-nitropropionic acid. *Neuroscience*. 1997;79(1):45–56.
30. Ludolph AC, He F, Spencer PS, Hammerstad J, Sabri M. 3-Nitropropionic acid-exogenous animal neurotoxin and possible human striatal toxin. *Can J Neurol Sci*. 1991;18(4):492–498.
31. Yamaguchi H, et al. MTH1, an oxidized purine nucleoside triphosphatase, protects the dopamine neurons from oxidative damage in nucleic acids caused by 1-methyl-4-phenyl-1,2,3,6-tetrahydropyridine. *Cell Death Differ.* 2006;13(4):551–563.
32. Ohno M, Oka S, Nakabeppu Y. Quantitative analysis of oxidized guanine, 8-oxoguanine, in mitochondrial DNA by immunofluorescence method. *Methods Mol Biol.* 2009;554:199–212.
33. Alam TI, et al. Human mitochondrial DNA is packaged with TFAM. *Nucleic Acids Res*. 2003; 31(6):1640–1645.
34. Oka S, Ohno M, Tsuchimoto D, Sakumi K, Furuichi M, Nakabeppu Y. Two distinct pathways of cell death triggered by oxidative damage to nuclear and mitochondrial DNAs. *EMBO J*. 2008; 27(2):421–432.
35. Czogalla A, Sikorski AF. Spectrin and calpain: a 'target' and a 'sniper' in the pathology of neuronal cells. *Cell Mol Life Sci*. 2005;62(17):1913–1924.
36. Brouillet E, Jacquard C, Bizat N, Blum D. 3-Nitropropionic acid: a mitochondrial toxin to uncover physiopathological mechanisms underlying striatal degeneration in Huntington's disease. *J Neurochem*. 2005;95(6):1521–1540.

37. Geddes JW, Bondada V, Tekirian TL, Pang Z, Siman RG. Perikaryal accumulation and proteolysis of neurofilament proteins in the post-mortem rat brain. *Neurobiol Aging*. 1995;16(4):651–660.
38. Hong SJ, Dawson TM, Dawson VL. Nuclear and mitochondrial conversations in cell death: PARP-1 and AIF signaling. *Trends Pharmacol Sci*. 2004; 25(5):259–264.
39. Ullrich O, Diestel A, Eyüpoglu IY, Nitsch R. Regulation of microglial expression of integrins by poly(ADP-ribose) polymerase-1. *Nat Cell Biol.* 2001; 3(12):1035–1042.
40. Ichikawa J, et al. Oxidation of mitochondrial deoxynucleotide pools by exposure to sodium nitroprusside induces cell death. *DNA Repair*. 2008; 7(3):418–430.
41. Oka S, Nakabeppu Y. DNA glycosylase encoded by *MUTYH* functions as a molecular switch for programmed cell death under oxidative stress to suppress tumorigenesis. *Cancer Sci.* 2011;102(4):677–682.
42. Yoshimura D, et al. An oxidized purine nucleoside triphosphatase, MTH1, suppresses cell death caused by oxidative stress. *J Biol Chem*. 2003; 278(39):37965–37973.
43. Kajitani K, Yamaguchi H, Dan Y, Furuichi M, Kang D, Nakabeppu Y. MTH1, an oxidized purine nucleoside triphosphatase, suppresses the accumulation of oxidative damage of nucleic acids in the hippocampal microglia during kainate-induced excitotoxicity. *J Neurosci*. 2006;26(6):1688–1698.
44. Imam SZ, Karahalil B, Hogue BA, Souza-Pinto NC, Bohr VA. Mitochondrial and nuclear DNA-repair capacity of various brain regions in mouse is altered in an age-dependent manner. *Neurobiol Aging*. 2006;27(8):1129–1136.
45. Kawarada Y, Miura N, Sugiyama T. Antibody against single-stranded DNA useful for detecting apoptotic cells recognizes hexadeoxynucleotides with various base sequences. *J Biochem*. 1998;123(3):492–498.
46. Ryu JK, Nagai A, Kim J, Lee MC, McLarnon JG, Kim SU. Microglial activation and cell death induced by the mitochondrial toxin 3-nitropropionic acid: in vitro and in vivo studies. *Neurobiol Dis*. 2003; 12(2):121–132.
47. Lin MT, Beal MF. Mitochondrial dysfunction and oxidative stress in neurodegenerative diseases. *Nature*. 2006;443(7113):787–795.
48. Block ML, Zecca L, Hong JS. Microglia-mediated neurotoxicity: uncovering the molecular mechanisms. *Nat Rev Neurosci*. 2007;8(1):57–69.
49. Vosler PS, Brennan CS, Chen J. Calpain-mediated signaling mechanisms in neuronal injury and neurodegeneration. *Mol Neurobiol*. 2008;38(1):78–100.
50. Nakabeppu Y, Tsuchimoto D, Yamaguchi H, Sakumi K. Oxidative damage in nucleic acids and Parkinson's disease. *J Neurosci Res*. 2007;85(5):919–934.
51. Hirano S, et al. Mutator phenotype of MUTYH-null mouse embryonic stem cells. *J Biol Chem*. 2003; 278(40):38121–38124.
52. Nishioka K, et al. Expression and differential intracellular localization of two major forms of human 8-oxoguanine DNA glycosylase encoded by alternatively spliced *OGG1* mRNAs. *Mol Biol Cell*. 1999;10(5):1637–1652.
53. Ohtsubo T, et al. Identification of human MutY homolog (hMYH) as a repair enzyme for 2-hydroxyadenine in DNA and detection of multiple forms of hMYH located in nuclei and mitochondria. *Nucleic Acids Res*. 2000;28(6):1355–1364.
54. Naruse I, Keino H, Kawarada Y. Antibody against single-stranded DNA detects both programmed cell death and drug-induced apoptosis. *Histochemistry*. 1994;101(1):73–78.
55. Tsuruya K, et al. Accumulation of 8-oxoguanine in the cellular DNA and the alteration of the OGG1 expression during ischemia-reperfusion injury in the rat kidney. *DNA Repair*. 2003;2(2):211–229.
56. Franklin KBJ, Paxinos G. *The Mouse Brain In Stereotaxic Coordinates*. San Diego, California, USA: Academic Press; 1997.
57. Iyama T, Abolhassani N, Tsuchimoto D, Nonaka M, Nakabeppu Y. NUDT16 is a (deoxy)inosine diphosphatase, and its deficiency induces accumulation of single-strand breaks in nuclear DNA and growth arrest. *Nucleic Acids Res*. 2010;38(14):4834–4843.
58. Tsuchimoto D, et al. Human APE2 protein is mostly localized in the nuclei and to some extent in the mitochondria, while nuclear APE2 is partly associated with proliferating cell nuclear antigen. *Nucleic Acids Res*. 2001;29(11):2349–2360.